TKK Dissertations 66
Espoo 2007

GROWTH AND IN SITU CHARACTERISATION OF DILUTE NITRIDE QUANTUM WELL STRUCTURES

Doctoral Dissertation

Outi Reentilä

Helsinki University of Technology
Department of Electrical and Communications Engineering
Micro and Nanosciences Laboratory

TKK Dissertations 66
Espoo 2007

GROWTH AND IN SITU CHARACTERISATION OF DILUTE NITRIDE QUANTUM WELL STRUCTURES

Doctoral Dissertation

Outi Reentilä

Dissertation for the degree of Doctor of Science in Technology to be presented with due permission of the Department of Electrical and Communications Engineering for public examination and debate in Large Seminar Hall of Micronova at Helsinki University of Technology (Espoo, Finland) on the 13th of April, 2007, at 12 noon.

Helsinki University of Technology
Department of Electrical and Communications Engineering
Micro and Nanosciences Laboratory

Teknillinen korkeakoulu
Sähkö- ja tietoliikennetekniikan osasto
Mikro- ja nanotekniikan laboratorio

Distribution:
Helsinki University of Technology
Department of Electrical and Communications Engineering
Micro and Nanosciences Laboratory
P.O. Box 3500
FI - 02015 TKK
FINLAND
URL: http://www.micronova.fi/units/oeg/
Tel. +358-9-4511
Fax +358-9-451 3128
E-mail: outi.reentila@tkk.fi

© 2007 Outi Reentilä

ISBN 978-951-22-8730-7
ISBN 978-951-22-8731-4 (PDF)
ISSN 1795-2239
ISSN 1795-4584 (PDF)
URL: http://lib.tkk.fi/Diss/2007/isbn9789512287314/

TKK-DISS-2281

Otamedia Oy
Espoo 2007

HELSINKI UNIVERSITY OF TECHNOLOGY P. O. BOX 1000, FI-02015 TKK http://www.tkk.fi	ABSTRACT OF DOCTORAL DISSERTATION
Author Outi Reentilä	

Name of the dissertation
Growth and optical in situ characterisation of dilute nitride quantum well structures

Date of manuscript 18th January 2007	Date of the dissertation 13th April 2007
☐ Monograph	☒ Article dissertation (summary + original articles)

Department	Department of Electrical Engineering
Laboratory	Micro and Nanosciences Laboratory
Field of research	Optoelectronics
Opponent(s)	Prof. Mattias Hammar
Supervisor	Docent Markku Sopanen

Abstract

In this work epitaxial growth and in situ characterisation of dilute nitride quantum well (QW) structures are studied. Dilute nitrides are III-V compound semiconductors with low (typically $< 5\%$) composition of nitrogen in the lattice. Metal organic vapor phase epitaxial (MOVPE) system was used to grow the structures and in situ reflectance monitoring in normal incidence at a wavelength of 635 nm was utilised to study the growth process of the structures. Ex situ characterisation was performed by x-ray diffractometry and photoluminescence measurements.

The nitrogen content of (In)GaAsN was found to depend on many MOVPE growth parameters. Increased nitrogen content was obtained with decreasing growth temperature, increasing DMHy/V and TBAs/III ratios and when nitrogen (N_2) was used as a carrier gas instead of hydrogen (H_2).

In situ reflectance data was measured during growth of GaAsN/GaAs, InGaAs/GaAs and InGaAsN/GaAs multi quantum well (MQW) structures. The reflectance curve was observed to be different when MQW structures with different compositions were grown. The reflectance data was analysed by an experimental method utilising the dependence of the reflectance change observed during growth of the QW on the QW composition. Additionally, reflectance curves for multi layer stacks were calculated and the measured curves were compared to the calculated ones. With both methods the sample composition can be determined *in situ* if the growth rates of the layers are known.

In the process of comparing calculated and measured reflectance curves, the high temperature complex refractive indices of the various QW materials were obtained. The imaginary part of the complex refractive index of (In)GaAsN was found to be linearly dependent on the nitrogen content, as well as both real and imaginary parts of the complex refractive index of InGaAs depended linearly on the indium content. However, changing the nitrogen content did not change the real part of the complex refractive index of (In)GaAsN.

The in situ analysis methods of MQW structures developed in this work can be used to obtain information about the growth process as well as about the materials themselves.

Keywords MOVPE, epitaxy, quantum wells, in situ monitoring, dilute nitrides

ISBN (printed) 978-951-22-8730-7	ISSN (printed) 1795-2239
ISBN (pdf) 978-951-22-8731-4	ISSN (pdf) 1795-4584
ISBN (others)	Number of pages 62+40

Publisher TKK Micro and Nanosciences Laboratory

Print distribution TKK Micro and Nanosciences Laboratory

☒ The dissertation can be read at http://lib.tkk.fi/Diss/2007/isbn9789512287314/

TEKNILLINEN KORKEAKOULU PL 1000, 02015 TKK http://www.tkk.fi	VÄITÖSKIRJAN TIIVISTELMÄ

Tekijä Outi Reentilä

Väitöskirjan nimi

Typpeä sisältävien kvanttikaivorakenteiden valmistus ja optinen in situ -karakterisointi

Käsikirjoituksen jättämispäivämäärä 18.1. 2007	Väitöstilaisuuden ajankohta 13.4. 2007
☐ Monografia	☒ Yhdistelmäväitöskirja (yhteenveto + erillisartikkelit)

Osasto	Sähkö- ja tietoliikennetekniikan osasto
Laboratorio	Mikro- ja nanotekniikan laboratorio
Tutkimusala	Optoelektroniikka
Vastaväittäjä(t)	Prof. Mattias Hammar
Työn valvoja	Dosentti Markku Sopanen

Tiivistelmä

Tässä väitöstyössä tutkittiin typpeä sisältävien kvanttikaivorakenteiden epitaktista valmistusta ja karakterisointia *in situ*. Rakenteet valmistettiin käyttäen metallo-orgaanista kaasufaasiepitaksiaa (engl. metal organic vapor phase epitaxy, MOVPE) ja valmistuksenaikainen tarkkailu toteutettiin MOVPE-laitteeseen kytketyllä kohtisuoran heijastuksen mittauslaitteistolla käyttäen 635 nm aallonpituutta. Valmistuksen jälkeisessä rakenteiden karakterisoinnissa käytettiin röntgendiffraktio- ja fotoluminesenssimittauksia.

Monien valmistusparametrien havaittiin vaikuttavan näytteiden typpipitoisuuteen MOVPE-prosessin aikana. Matalassa lämpötilassa valmistettujen näytteiden typpipitoisuus havaittiin suuremmaksi kuin korkeassa lämpötilassa valmistettujen näytteiden. Samaten DMHy/V-suhteen suurentaminen ja TBAs/III-suhteen suurentaminen kasvattivat typpipitoisuutta. Typpipitoisuuden havaittiin olevan suurempi näytteissä, joiden valmistuksessa oli käytetty typpeä (N_2) kantajakaasuna vedyn (H_2) sijaan.

GaAsN/GaAs, InGaAs/GaAs ja InGaAsN/GaAs monikvanttikaivorakenteiden (engl. multi quantum well, MQW) valmistusta tarkkailtiin heijastusmittauksin. Heijastuskäyrän havaittiin muuttuvan näytteiden koostumuksen muuttuessa. Heijastusdata analysoitiin käyttämällä kokeellista menetelmää, joka hyödyntää kvanttikaivon valmistuksenaikaisen heijastusmuutoksen ja kaivon koostumuksen välistä yhteyttä. Tämän lisäksi usean kerroksen rakenteille laskettiin heijastuskäyriä ja verrattiin niitä mitattuihin käyriin. Molemmilla metodeilla voidaan määrittää kvanttikaivon koostumus, mikäli kerrosten kasvunopeudet tunnetaan.

Laskettuja ja mitattuja heijastuskäyriä vertailemalla saatiin selvitettyä kvanttikaivomateriaalien kompleksiset taitekertoimet valmistuslämpötilassa. (In)GaAsN:n kompleksisen taitekertoimen imaginaariosan havaittiin muuttuvan lineaarisesti typpipitoisuuden funktiona, kuten myös InGaAs:n kompleksisen taitekertoimen reaali- ja imaginaariosat riippuivat lineaarisesti indiumpitoisuudesta. Typpipitoisuuden muutoksen ei kuitenkaan havaittu vaikuttavan (In)GaAsN:n reaaliosaan.

Tässä työssä kehitetyillä MQW-rakenteiden in situ -karakterisointimenetelmillä voidaan saada tietoa valmistusprosessista sekä valmistettavasta materiaalista itsestään.

Asiasanat MOVPE, epitaksia, kvanttikaivo, valmistuksenaikainen tarkkailu, laimeat nitridit

ISBN (painettu) 978-951-22-8730-7	ISSN (painettu) 1795-2239
ISBN (pdf) 978-951-22-8731-4	ISSN (pdf) 1795-4584
ISBN (muut)	Sivumäärä 62+40

Julkaisija TKK Mikro- ja nanotekniikan laboratorio

Painetun väitöskirjan jakelu TKK Mikro- ja nanotekniikan laboratorio

☒ Luettavissa verkossa osoitteessa http://lib.tkk.fi/Diss/2007/isbn9789512287314/

Preface

The work presented in this thesis was carried out in the Optoelectronics and Micro and Nanosciences Laboratories at Helsinki University of Technology during 2004-2007. I want to express my great gratitude to Professor Harri Lipsanen for the opportunity to work in the field of semiconductor fabrication and for the support during this time.

I am deeply grateful to Docent Markku Sopanen, the supervisor of this thesis, for his continuous support and interest in my work as well as for the numerous times of guidance and conversation. I want to thank M. Sc. Marco Mattila, not only for the collaboration in the growth and characterisation during the work, but also for the interesting and fruitful conversations over the years. I am grateful to Dr. Lauri Knuuttila for the collaboration in MOVPE growth and Dr. Teppo Hakkarainen for his input in the writing process. And last but not least, I would like to thank the personnel of the Laboratory for all the help I have got and for the enjoyable working atmosphere.

The National Graduate School of Material Physics, Tekniikan edistämissäätiö and Jenny ja Antti Wihurin rahasto are gratefully acknowledged for their financial support of my work.

I want to express my great gratitude to my parents Ulla and Matti and to my brother Osmo for their love and continuous encouragement. I also want to thank all my dear friends, especially Laura, Sanna and Nippe, for the support I have always had and for the activities which made me forget about the work – at least for a while. Finally, I would like to thank my boyfriend Jaakko for all the understanding encouragement and for all the hugs.

Espoo, January 2007

Outi Reentilä

Table of contents

Preface **vii**

Table of contents **viii**

List of publications **ix**

Author's contribution **x**

1 Introduction **1**

2 Dilute nitrides **4**
2.1 Compound semiconductors 4
2.2 Effect of nitrogen on bandgap 6
2.3 Material quality related issues 8
2.4 Applications of dilute nitrides 11

3 Experimental **12**
3.1 Metal organic vapour phase epitaxy 12
3.2 Optical in situ monitoring system 14
3.3 X-ray diffractometry 16
3.4 Photoluminescence spectroscopy 18

4 MOVPE growth parameter optimisation for InGaAsN **19**
4.1 Growth and annealing temperatures 19
4.2 Precursor molar flows 20
4.3 Choice of carrier gas 23

5 Calculation and simulation of reflectance curves **26**
5.1 Theoretical calculation of in situ reflectance curve 26
5.2 Simulation of reflectance data 29

6 Determination of dilute nitride QW composition and quality by optical in situ monitoring **34**
6.1 Slope method 34
6.2 Experimental data and matrix method 37
6.3 Observing layer quality during growth 43

7 Summary **45**

List of publications

This thesis consists of an overview and of the following publications which are referred to in the text by their Roman numerals.

I O. Reentilä, M. Mattila, M. Sopanen, and H. Lipsanen, *Nitrogen content of GaAsN quantum wells by in-situ monitoring during MOVPE growth*, Journal of Crystal Growth **290** 345–349 (2006)

II O. Reentilä, M. Mattila, L. Knuuttila, T. Hakkarainen, M. Sopanen, and H. Lipsanen, *In situ determination of nitrogen content in InGaAsN quantum wells*, Journal of Applied Physics **100** 013509 (2006)

III O. Reentilä, M. Mattila, L. Knuuttila, T. Hakkarainen, M. Sopanen, and H. Lipsanen, *Comparison of H_2 and N_2 as carrier gas in MOVPE growth of InGaAsN quantum wells*, Journal of Crystal Growth **298** 536–539 (2007)

IV O. Reentilä, M. Mattila, M. Sopanen, and H. Lipsanen, *In-situ determination of InGaAs and GaAsN composition in multi-quantum-well structures*, Journal of Applied Physics **101** 033533 (2007)

V O. Reentilä, M. Mattila, M. Sopanen, and H. Lipsanen, *Simultaneous determination of indium and nitrogen contents of InGaAsN quantum wells by optical in-situ monitoring*, Applied Physics Letters **89** 231919 (2006)

VI L. Knuuttila, O. Reentilä, M. Mattila, and H. Lipsanen, *Comparison of Ge and GaAs substrates for metalorganic vapor phase epitaxy of GaIn(N)As quantum wells*, Japanese Journal Applied Physics **44** L1475–L1477 (2005)

Author's contribution

The sample structures and experimental procedures for all the publications were planned and realized by the author and the co-authors.

All the manuscripts except for the manuscript of publication VI have been written by the author. The intepretation of the results of publications I- V has been performed mainly by the author with help from M. Mattila. For publication VI the author has participated in the interpretation of the results.

The author has grown the samples for publications IV and V. The samples for publications I, II and III were fabricated by the author and M. Mattila. For publication VI the samples were fabricated by L. Knuuttila with a small contribution from the author.

The photoluminescence measurements for publications I, III, IV and V were performed by the author. For publication II the photoluminescence measurements were performed by the author and M. Mattila together and for VI by L. Knuuttila.

The x-ray diffraction characterization of publications II and IV was carried out by the author and M. Mattila together. For publications I and V the x-ray diffraction measurements were performed by M. Mattila. The author has participated in the simulation of the measured data. The x-ray characterization for publication VI was carried out by L. Knuuttila.

1 Introduction

Optoelectronics is a research field, which deals with the interaction of light and the electronic structure of materials. Typical optoelectronic components can generate light out of electricity, like semiconductor lasers and light emitting diodes (LEDs), or *vice versa*, electric current from light input, like solar cells and optical detectors. These days applications of optoelectronic components as such or as a part of larger systems can be found from a variety of technogical sectors.

Traditional semiconductor components, such as edge emitting lasers and LEDs, consist of thick bulk layers fabricated on top of each other. Typical fabrication methods are liquid phase epitaxy (LPE), metal organic vapour phase epitaxy (MOVPE) and molecular beam epitaxy (MBE). However, modern semiconductor components tend to take full advantage of the possibilities of low dimensional structures. The fabrication of such structures is complicated and dedicated fabrication processes need to be applied. MOVPE and MBE systems can be used to fabricate quantum dots, quantum wires and quantum wells (QWs) as well as bulk layers of semiconductors. As the growth processes get more complicated, the demand of accuracy is also increasing. This requires the development of advanced in situ characterisation techniques.

In the recent decades in situ monitoring of the epitaxial growth processes has proven to be a useful tool to improve the quality and yield of the growth process [1]. In MBE systems the in situ monitoring is often realised with the reflection high energy electron diffraction (RHEED) method, which cannot be applied to MOVPE processes because RHEED operates only in vacuum. However, MOVPE growth of III-V semiconductors can be monitored using several different optical monitoring techniques. Such methods are for example reflectance anisotropy spectroscopy (RAS), ellipsometric spectroscopy (ES) and reflectance measurements.

This study concentrates on the reflectance in situ monitoring of MOVPE growth. Typically, in situ reflectance monitoring has been applied to growth of either a GaN related material or a bulk III-V semiconductor structure. In order to grow GaN related materials, the information provided by in situ monitoring is crucial because of the rather complicated growth procedure of GaN on sapphire substrates [2]. In situ monitoring of Bragg mirror structures has also proven to be very useful in order to maximise the reflectance of the mirror by means of measuring the layer

thicknesses *in situ* [3, 4]. The thicknesses or high temperature optical constants of thick layers other than binary alloys, for example AlGaAs, InAlAs, InGaAsP and AlGaInP can be measured easily using in situ reflectometry [5–7]. In addition, by choosing a suitable wavelength, even the reflectance of the mirror at its operational wavelength can be measured [8].

The optical in situ monitoring of QW growth has not been studied extensively to date. Reports of Lum *et al.* [9], Zorn *et al.* [10] and Wolfram *et al.* [11] show that growth of thin QW layers can be resolved if the monitoring wavelength is chosen correctly. However, despite the fact that the growth regions of QWs can be distinguished, an in situ study of the properties of the QWs has not been performed.

QWs are used as the active part of several components, for example, vertical cavity surface emitting lasers (VCSELs) and semiconductor saturable absorber mirrors (SESAMs). For components operating at optical telecommunication wavelengths 1300 nm and 1550 nm a material with a suitable bandgap is required. Such a bandgap can be realised with InP based materials. Also alloy semiconductors, which contain a low concentration of nitrogen, *i.e.*, dilute nitrides, have been proposed as candidates for active material of components operating at 1300 nm and 1550 nm [12]. Therefore, dilute nitrides have been studied extensively over the past decade, see Ref. 13 and references therein. The main advantage of the dilute nitride InGaAsN over InP based materials is the possibility to grow it directly on a GaAs substrate and, thus, utilise GaAs processing technology and GaAs based Bragg reflectors.

It is clear from the dilute nitride studies that the fabrication conditions of dilute nitrides tend to differ from the epitaxial processes used to grow many other materials and that the growth conditions for dilute nitrides have to be carefully optimised for nitrogen incorporation. Using in situ monitoring equipment helps to optimise the growth conditions but it also provides information about the material. The information obtained during growth can be of such nature, that it is challenging to achieve by ex situ measurements. Additionally, for component fabrication the in situ monitoring of the QWs within the component structure might be the simplest way to study the thin layers in detail, because after growth the measurement of such a complicated structure is difficult.

This thesis discusses the in situ reflectance measurements of (In)GaAs(N) MQW structures with various compositions. The possibility to determine the QW composition *in situ* has been studied. First an experimental method, called the slope method, was developed. It utilises the relation between the sample composition and the reflectance change observed during growth of the first QW of the structure. To further improve the analysis process of the in situ reflectance data, matrix method was used to calculate theoretical reflectance curves for MQW structures. The theoretical curves were compared to the measured data and as a result the high temperature complex refractive index of the QW material was obtained as a function of the composition. When the complex refractive indices and the growth

rates of all the layers are known at the growth temperature, the layer compositions for the MQW structure can be resolved *in situ*.

The structure of the overview of this thesis is as follows. Chapter 2 gives a short introduction into alloy semiconductors and into dilute nitrides as a material group. Chapter 3 outlines the fabrication and characterisation techniques used. Chapter 4 discusses MOVPE growth of dilute nitrides and summarises the growth process optimisation results from publications I, II, III and VI. Chapter 5 introduces the matrix model utilised to analyse the in situ data. The analysis performed on the in situ data is discussed in Chapter 6. Section 6.1 describes the results obtained using the slope method and summarises the in situ results of publications I, II and III, whereas Section 6.2 presents the results obtained by the application of the matrix method from publications IV and V. Finally, Chapter 7 summarises the main results of this thesis.

2 Dilute nitrides

This chapter gives a brief introduction into compound semiconductors and dilute nitrides. First, Section 2.1 introduces compound semiconductors and some basic concepts relevant for this thesis. In Section 2.2 the effect of nitrogen on the bandgap of dilute nitrides is discussed, and in Section 2.3 an insight into issues related to material quality is given. Finally, Section 2.4 discusses the applications and future possibilities of dilute nitrides.

2.1 Compound semiconductors

Materials can be divided into metals, semiconductors and insulator on the grounds of their electrical conductivity. The electrical conductivity is determined by the existence and the width of the bandgap in the material. The bandgap divides the band structure into separate conduction and valence bands. Only the electrons lying in the conduction band and the holes in the valence band can move and, thus, conduct current. Because of that they are called charge carriers. Metals do not have a bandgap and, thus, all the free outer shell electrons can carry current. In insulators the bandgap is so wide that only an insignificant concentration of electrons is thermally activated at room temperature. In semiconductors the bandgap is between these two cases and a considerable concentration of electrons can be excited to the conduction band by thermal energy at room temperature. The excitation of an electron leaves also a vacancy called a hole in the valence band. Because the bandgap determines many properties of the semiconductor, for example its operational wavelength and its ability to handle high voltage, it is a very crucial parameter when semiconductors are considered.

Semiconductors can be divided into elemental semiconductors and compound semiconductors. Elemental semiconductors are materials, which have atoms of only one element, for example, germanium and silicon. Compound semiconductors, on the other hand, are materials, which have a combination of atoms from two or more different groups of the periodic table in one lattice, for example GaAs (from groups III and V) and ZnSe (from groups II and VI).

Compound semiconductors can be used to form alloys of more than two components.

Materials having three components are called ternary alloys and materials with four components are quaternary alloys. Examples of such alloys are AlGaAs (from groups III, III and V) and InGaAsN (III-III-V-V). Alloying materials is easiest when the sizes and the electronegativities of the atoms from the same elemental group are close to each other, as for example is the case for AlGaAs.

The characteristics of the ternary and quaternary semiconductor alloys are usually determined by the composition of the material. Furthermore, the characteristics are typically changing smoothly as a function of the composition if any critical points, such as a transition from direct to indirect bandgap, are not present. For example, the lattice constant of the ternary alloy is described by Vegard's law, which is a linear approximation between the lattice constants of the constituting binary compounds of the ternary alloy. However, the bandgap energy of a ternary alloy $A_{\mathrm{x}}B_{1-\mathrm{x}}C$ can be written

$$E_{\mathrm{g,ABC}} = x \cdot E_{\mathrm{g,AC}} + (x-1) \cdot E_{\mathrm{g,BC}} - x(1-x)b_{\mathrm{ABC}} \qquad (2.1)$$

where x is the proportion of element A in ABC, $E_{\mathrm{g,AC}}$ and $E_{\mathrm{g,BC}}$ are the bandgaps of the binary alloys AC and BC and b_{ABC} is the bowing parameter. The bowing parameter describes the deviation of the bandgap energy from the linear approximation. Calculation of the bandgap of a typical quaternary alloy is usually performed using a numerical expression individual to each alloy.

Modern semiconductor technology enables fabrication of complicated materials in complicated structures. Heterostructures are systems where two or more different materials are grown on each other, for example InGaAs on GaAs. In an ideal heteroepitaxial growth process the single crystalline layer copies the substrate lattice constant in the surface plane. This is a very unique phenomenon and separates epitaxial processes from other thin film deposition methods. The thickness of the epitaxial layer can be varied from a few nanometers to micrometers depending on the material combination and the growth method.

Some epitaxial methods are well suitable for fabricating nanoscale semiconductor structures like, for example, quantum wells (QWs). Quantum wells are technologically interesting due to their large potential in many applications. QW is a structure where a thin layer of material with a small bandgap is sandwiched between a large bandgap material. The QW needs to be thin enough so that the electronic states of the carriers are quantised in the direction perpendicular to the QW plane.

Dilute nitrides are III-V semiconductor alloy materials, which contain a small concentration of nitrogen. Dilute nitrides differ somewhat from the typical III-V semiconductors by their properties and behaviour. This is caused by the large difference in the electronegativity and size between nitrogen and the other group V atoms used

in compound semiconductors (usually arsenic or phosphorus). Typically, the host material into which nitrogen is incorporated is GaAs or InGaAs leading to dilute nitride alloys GaAsN and InGaAsN. However, also studies of GaPN [13–15], InPN [16], AlGaAsN [17] and GaAsPN [18] have been reported. Usually the nitrogen content is less than 5 %, but there are reports of nitrogen contents of as high as 9.6 % and 14 % in GaAsN [19–21].

2.2 Effect of nitrogen on bandgap

The band structure and the bandgap energy are important factors when semiconductors are considered. Typically, the bandgap of a ternary alloy semiconductor can be quite well estimated by Eq. 2.1. Additionally, the effect of the term containing the bowing parameter b is relatively small. Usually the value of the bowing parameter is less than 1 eV, even though for some antimonide alloys it is as high as 2.7 eV (GaPSb, AlPSb) [22].

The bandgap of dilute nitrides decreases drastically when the nitrogen content of the material increases. If the band bowing would be neglected, the bandgap of GaAsN should be increasing with increasing nitrogen content, as the bandgaps of GaAs and cubic GaN are 1.519 eV and 3.299 eV, respectively [22]. However, the bowing parameter of dilute nitride alloys is large, *e.g.*, for GaAsN it is approximately 14-26 eV, see for example Refs. 21 and 24-26. In addition, several studies suggest that the bowing parameter of GaAsN is dependent on the nitrogen content [20, 22–24]. Typically dilute nitride alloys containing less than 1 % of nitrogen are considered to have a low nitrogen content. A nitrogen content larger than that is typically considered high.

Fig. 2.1 shows the bandgap energy as a function of the GaAsN QW nitrogen content for some of the samples fabricated for this thesis. The quantisation of the energy levels in QWs has been neglected. The bowing parameter derived from the GaAsN samples was 14 eV. It should be noted that the nitrogen contents of the samples are rather high, which lead to a smaller bowing parameter than what has been observed for low nitrogen contents (1 % or less). Nevertheless, a good agreement with the results from similar nitrogen contents reported by others (see Refs. above) was achieved. The inset of Fig. 2.1 shows the bandgap energy of GaAsN as a function of the nitrogen content over the whole nitrogen content range from GaAs to cubic GaN calculated by using the bowing parameter value of 14 eV. The calculation leads to unphysical negative value of the bandgap in the nitrogen content range of 15-70 %, indicating that the value $b = 14$ eV does not apply for the whole range and that the bowing parameter indeed has to be composition dependent.

The effect of nitrogen on the band structure of (In)GaAsN is complicated. Several models have been introduced to explain the behaviour of the band gap energy and

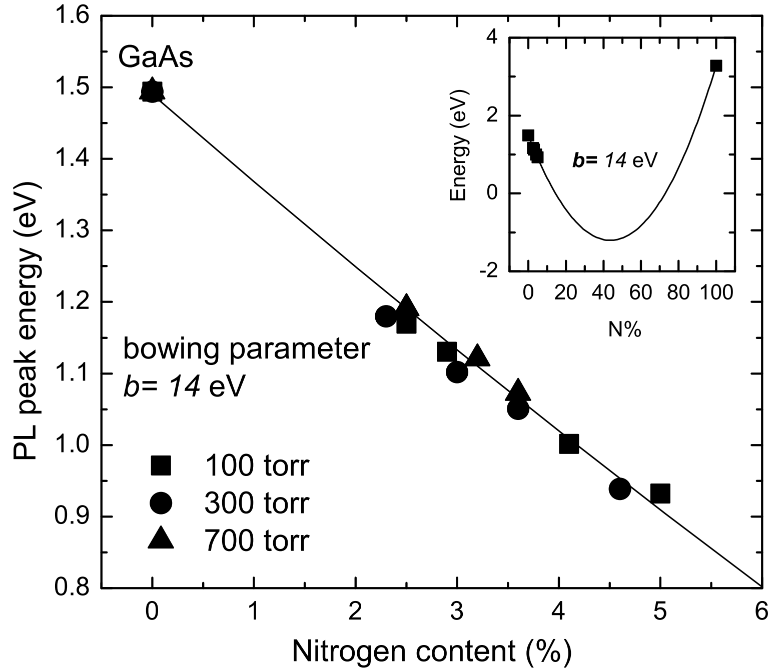

Figure 2.1: LTPL peak energy as a function of GaAsN nitrogen content. The inset shows the bandgap (calculated with $b = 14$ eV) over the whole nitrogen content range from GaAs to cubic GaN.

to describe the band structure of (In)GaAsN as a function of the nitrogen content. Dedicated (In)GaAsN models are required, because models typically used for alloy semiconductors, *e.g.*, virtual-crystal approximation (VCA), do not hold for dilute nitrides. This is because the addition of nitrogen atoms causes large perturbation in the lattice due to the large difference in size and electronegativity between the nitrogen and the arsenic atoms. Models used to calculate the band structure of (In)GaAsN are, for example, the band anti-crossing (BAC) model [25–27], large supercell empirical pseudopotential method (EPM) [28, 29] and extended ten-band $\mathbf{k}\cdot\mathbf{p}$ model using the tight-binding Hamiltonian [30].

The BAC model is a simple method to describe the influence of nitrogen on the band structure of (In)GaAsN. When nitrogen is added to (In)GaAs, a nitrogen related perturbation level appears inside the conduction band, near the conduction band edge [31]. In the BAC model, the interaction between the nitrogen resonance level (E_N) and the unperturbed semiconductor states (E_M) leads to splitting of the conduction band into two subbands, E_+ and E_-, because the conduction band states

are not allowed to cross the perturbation level. The interaction between the nitrogen related perturbation and the unperturbed states gets stronger with increasing nitrogen content. The subband E_- is pushed into the bandgap and the strong reduction of the bandgap energy can be observed. In this study, the relationship given by the BAC model between (In)GaAsN nitrogen content and the bandgap energy is used in the process of InGaAsN nitrogen content determination. The x-ray diffraction and photoluminescence results were employed to determine the nitrogen concentration together with the BAC model simulations.

Generally in III-V semiconductors, both conduction and valence bands are affected by alloying. In the case where the valence band maximum of the layer is at a higher energy and the conduction band minimum is at lower energy than those of the host material, the band alignment is called to be of type I. If both the valence band maximum and the conduction band minimum are located either at a higher or at a lower level of energy than those of the adjacent material, the band alignment is called to be of type II. QWs have type I band alignment, and type I is preferable for optically active components, because the both types of the carriers are confined in the same volume.

In GaAsN the distribution of the band offset respective to GaAs is expected to be concentrated strongly into the conduction band [32]. Although nitrogen creates a resonant level near the conduction band edge, which causes the reduction of the bandgap, the valence band remains relatively unchanged. There has been a wide controversy about to which direction the valence band edge actually moves and publications supporting both type I [33, 34] and type II [35, 36] band alignment in GaAsN/GaAs structures exist. Intuitively type II would be logical, because the valence band maximum of cubic GaN is 1.84 eV lower than the valence band maximum of GaAs [37]. However, in the recent publications type I alignment is preferred [38], meaning that the valence band maximum of GaAsN is shifted upwards in energy compared to the valence band of GaAs. The band alignment of InGaAsN with respect to GaAs is type I because addition of indium into GaAs causes a relatively large increase in the valence band maximum.

2.3 Material quality related issues

Nitrogen has a strong effect on the material quality of the dilute nitride alloys. It is nowadays commonly known that incorporating nitrogen into (In)GaAs lattice decreases the material quality of dilute nitrides. This is demonstrated in Fig. 2.2, which shows low-temperature photoluminescence (LTPL) spectra of several GaAsN multi QW (MQW) samples that contain different amounts of nitrogen. It is apparent that as the nitrogen content increases the PL intensity decreases and also the full width half maximum (FWHM) of the peak increases, both indicating reduced material quality. The PL intensity of the $GaAsN_{0.023}$ sample is over 20 times larger

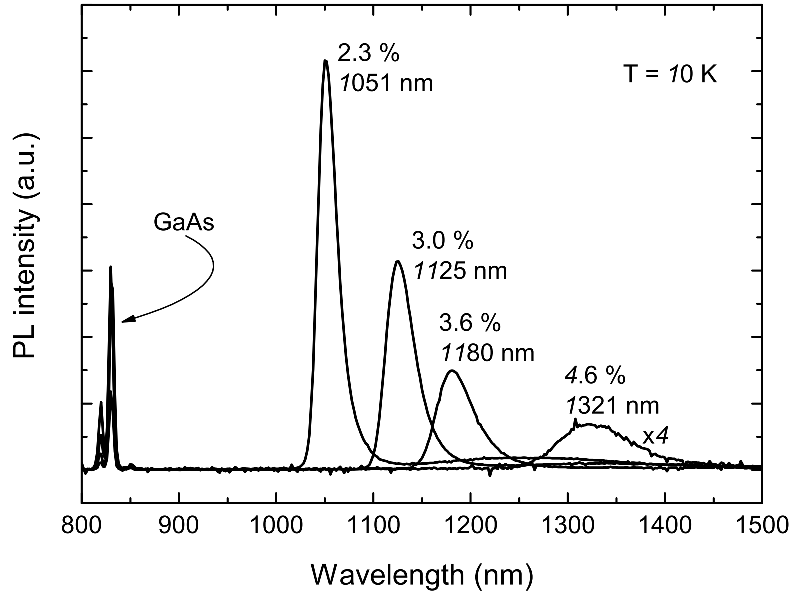

Figure 2.2: LTPL spectra measured from several annealed GaAsN MQW samples. The nitrogen content of each sample is denoted in the figure. The PL spectrum of the sample containing 4.6 % of nitrogen is multiplied by four for clarity.

than the intensity measured from the $GaAsN_{0.046}$ sample. Another direct indication of the reduced material quality is short minority carrier lifetimes observed in dilute nitrides [39, 40].

The defects in dilute nitrides have been studied extensively. Several specific defects have been found to form in dilute nitrides, for example, arsenic antisites [41], nitrogen split interstitials [42] and gallium vacancies (V_{Ga}) [43–45]. Furthermore, the number of gallium vacancies in (In)GaAsN has been observed to be considerably higher than the number observed in samples without nitrogen [43, 44]. The formation of the gallium vacancies has been explained by the strong binding of V_{Ga} to both nitrogen and hydrogen. The strong binding decreases the formation energy of the vacancies and, thus, increases their concentration in the dilute nitride material [46, 47]. Decrease in the hydrogen concentration reduces the V_{Ga} concentration, but still more work is needed to fully understand the formation and effects of V_{Ga} as well as the role of the other defects.

The incorporation of hydrogen into InGaAsN is an interesting phenomenon, which

has been widely studied. Increased hydrogen incorporation has been reported when nitrogen is present, see for example Refs. 48 and 49. It was also observed in Publication III by secondary ion mass spectrometry (SIMS) that hydrogen is incorporated considerably more into InGaAsN quantum wells than into GaAs barriers. Additionally, the incorporation of undesired hydrogen seems to be a problem related to MOVPE growth [48]. This can explained by the large amount of hydrogen present in the MOVPE growth process. Hydrogenation treatments have been performed on purpose and a decrease in photoluminescence wavelength of InGaAsN has been found with increasing hydrogen content [49]. However, the original PL characteristics can be restored if thermal annealing is used to remove the hydrogen atoms from the lattice. Janotti *et al.* have calculated that the redshift of the InGaAsN PL peak with increasing hydrogen concentration is caused by formation of charge neutral H_2^*N complexes [50].

Extensive amount of work has been carried out in order to improve the material quality after growth. Dilute nitrides are metastable materials. Metastability means that the lattice sites of the atoms are not stable and already small amount of energy can change the configuration of the material. Therefore, the characteristics of these materials can be affected after growth by using such methods as thermal annealing [51] and laser treatment [52]. Time, temperature and atmosphere have been found to influence the effect of the thermal annealing [53–55]. In general, annealing and laser treatment have been found to improve the characteristics of the dilute nitrides. For example, increase in the PL intensity has been observed. However, also a blueshift of the PL peak appears after the thermal treatment. The observation that the configuration of the lattice is changed by after growth treatments indicates that the material initially grows into an energetically unstable configuration [54, 56, 57].

The lattice sites of the nitrogen atoms in (In)GaAsN have been widely studied. Theoretical lattice energy calculations show that the most preferable place for a nitrogen atom in the InGaAsN lattice is where the nitrogen is surrounded by as many indium atoms as possible as the nearest neighbours [58, 59]. As a result of thermal annealing, the lattice is rearranged preferring such configuration. This is considered to be the possible reason for the blueshift as well as for the improved PL intensity of the photoluminescence peak of InGaAsN. However, because of optical quality and photoluminescence peak energy of GaAsN also change as a result of the thermal annealing treatment, the whole annealing behaviour of the material can not be explained by the relationship between indium and nitrogen which is not present in the GaAsN lattice. A definite explanation does not exist at this time, but studies indicate that hydrogen atoms incorporated into the lattice during the growth might play some role in the effects of the thermal annealing. Additionally, removal of gallium vacancies and nitrogen complexes from the lattice have been suggested as reasons for the enhanced luminescence intensity after annealing [42, 43, 47]. The final explanation will probably be a combination of several reasons, some of which might still be undiscovered.

2.4 Applications of dilute nitrides

Dilute nitrides are interesting materials for many applications. Both GaAsN and InGaAsN can be fabricated on GaAs substrates due to the small lattice mismatch and, therefore, existing GaAs processing technology can be used. For some components the possibility to use GaAs based Bragg reflectors is important. InGaAsN has a wide wavelength range and the telecommunication wavelengths 1.3 and 1.55 μm can be reached with a correct composition. The use of InGaAsN in several components has been reported, for example, in laser diodes [60], vertical cavity surface emitting lasers (VCSELs) [60–62], large area and ridge waveguide lasers [63], solar cells [64, 65] and semiconductor saturable absorber mirrors (SESAMs) [66, 67].

Two main issues have to be considered when light emitting dilute nitride components, such as VCSELs, operate at long wavelengths. First, the bandgap of the material needs to be tuned so that the operational wavelength of the component is correct. Secondly, the material quality has to be high in order to produce functional components. Both of these goals provide currently a challenge for epitaxy. The material quality related problems still limit the wide use of dilute nitrides in laser components.

Solar cells are components that convert light into current. Already one p-n junction can function as a solar cell. However, to fabricate more efficient components it is preferable to use many junctions made of different direct bandgap semiconductors. That way the energy is collected from a larger portion of the solar spectrum. The quaternary alloy InGaAsN is a good candidate for one layer of the four junction solar cell, because it can be fabricated lattice matched to GaAs and Ge and its bandgap can be tuned to 1.0 eV. However, the minority carrier lifetime of InGaAsN needs to be increased. The short minority carrier lifetimes reported for InGaAsN limit the diffusion length of the generated carriers in the material and, thus, prevent the effective operation of the solar cell [39, 40].

SESAMs are passive components that are used for mode locking and Q-switching of lasers. The material quality issue limiting the use of dilute nitrides in active components is not as serious when mode locking SESAMs are considered. In SESAMs the recovery of the carriers ought to be fast in order to obtain high repetition rates. The defects that nitrogen introduces to the material shorten the recovery time and, thus, fast SESAMs can be produced without any additional processing. In addition, because the lattice mismatch can be controlled by the adjustment of the indium and nitrogen contents, the number of QWs can be large and, consequently, the modulation depth of the component can be widely tuned. Some of the InGaAsN QW structures studied in this thesis were used as absorbing parts of SESAM devices. SESAM components were fabricated to operate at several wavelengths and operation has been demonstrated so far for 1064 nm and 1550 nm.

3 Experimental

Chapter 3 describes the experimental procedures of sample fabrication and characterisation. Section 3.1 introduces the metal organic vapour phase epitaxial system which was used to fabricate the samples. In Section 3.2 the optical in-situ monitoring system is described. Sections 3.3 and 3.4 introduce the x-ray diffraction and photoluminescence measurement systems, respectively, used for ex situ characterisation of the samples.

3.1 Metal organic vapour phase epitaxy

Compound semiconductor structures can be fabricated, *e.g.*, by metal organic vapour phase epitaxy (MOVPE) or molecular beam epitaxy (MBE). Sharp interfaces and high accuracy of composition can be obtained by both methods, which makes it possible to fabricate low dimensional structures. However, the two methods differ in how the atoms are guided onto the substrate surface where the actual growth occurs. In MBE systems an ultra high vacuum in the growth chamber is needed and elemental species are evaporated on the heated substrate. In MOVPE technique a carrier gas is used to transfer the precursor molecules into the reactor and onto the substrate surface.

An important factor in MOVPE growth is the control of the carrier gas. Fig. 3.1 shows a schematic diagram of the low pressure MOVPE gas system, which was used in this thesis. The typical choices for the carrier gas are hydrogen H_2 and nitrogen N_2, which both are easy to purify and do not significantly participate in the growth reactions. The ultra pure carrier gas is driven into bubblers, where the precursors are located. In MOVPE the precursors are typically liquid (some are solid) metal organic chemicals. The precursor molecules are saturated into the carrier gas and the saturation concentration is controlled by the temperature and the pressure of the bubbler. The control is achieved by placing the bubblers in temperature controlled baths and by using pressure controllers (PCs) in bubbler gas lines. The unsaturated carrier gas enters and the saturated carrier gas leaves the bubblers through mass flow controllers (MFCs), which make it possible to control the flows accurately. If very small concentrations of precursors are needed, an additional dilution flow can be used. The gas flow from the bubbler is directed to the reactor via gas lines. In

some systems multiple gas lines are used, for example, to separate group III and group V precursors from each other.

In the reactor high temperature of the heated susceptor cracks the precursor molecules. The metallic atoms and organic molecules from the decomposed metal organic molecules arrive to the substrate surface by gas phase diffusion. On the surface the atoms diffuse around in search of local energetic minima. The sticking coefficient is a factor describing the probability of the attaching of the atom. For efficient use of precursors, the sticking coefficient of the metal atoms should be close to one.

The growth temperature is an important parameter in MOVPE growth. The lower boundary of the possible temperature range in the MOVPE process is determined by the decomposition temperatures of the precursor molecules. For example, the precursor molecules for indium and arsenic, trimethylindium and tertiarybutylarsine, are fully decomposed at around 350°C and 400°C, respectively [68]. However, the temperature of full decomposition of trimethylgallium is as high as 470°C [69]. Additionally, the typical nitrogen precursor for dilute nitride growth, dimethylhydrazine is expected to be fully decomposed at 850°C, and about 50 % of DMHy molecules are decomposed at 550°C [70]. When considering the higher boundary of the growth temperature the desorption of the group V atoms from the surface needs to be taken into account. Additionally, at high temperature the bulk diffusion is increased which readily leads to mixing of the interfaces between the epitaxial layers.

The group III precursor molar flow affects the growth process in a different manner than the group V molar flow. Typically, the combined group III molar flow determines the growth rate at the mass transport limited growth temperature range [68]. Naturally, the thickness of each layer is determined by the growth time and the growth rate. In contrast, the group V molar flow has to be large enough so that the sample surface is protected from desorption of the group V atoms. The ratio of group V and group III molar flows is called V/III ratio. The V/III ratio influences the number of vacancies created and the possible deviation from stoichiometry, as well as, *e.g.*, the efficiency of the doping. The molar flow ratios within the group III or V are used to control the layer composition in ternary and quaternary materials.

The samples for this work were fabricated by two MOVPE systems. Most of the samples were fabricated with a low pressure (LP) close coupled showerhead (CCS) MOVPE system where the optical reflectance setup for in situ monitoring was attached. Fig. 3.1 shows the schematic diagram of the CCS system. The reactor is placed in a glove box having a nitrogen ambient to minimise contamination in the process. The gases arrive into the showerhead through two gas lines. The showerhead directs the gas flows to the susceptor and the gases carrying the group III and group V precursor molecules mix only after the showerhead. The use of showerhead design leads to more homogeneous growth profile and reduces the possibility of gas phase pre-reactions between the different precursors. The maximum amount of sub-

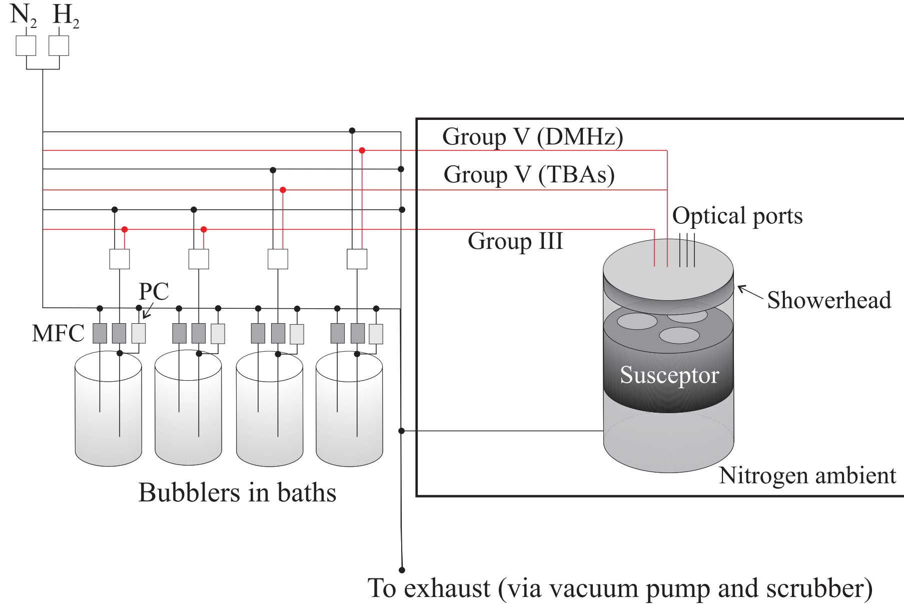

Figure 3.1: Schematic diagram of the low pressure CCS MOVPE system.

strates in one run is 3×2" wafers. A temperature range up to 1200°C and a pressure range of 50-800 torr are possible with the CCS system. The heating is realised with a resistive heater under the graphite susceptor. Trimethylindium (TMIn), trimethylgallium (TMGa), trimethylaluminium (TMAl) tertiarybutylarsine (TBAs) and dimethylhydrazine (DMHy) have been used as precursors for indium, gallium, aluminium, arsenic and nitrogen, respectively.

Some of the samples were grown (in publication VI) and some of the ex situ annealing treatments were performed at atmospheric pressure using a horizontal reactor MOVPE system having a maximum substrate size of 2×2 cm^2 and a temperature range up to 900°C. In this MOVPE system, an infrared lamp is used to heat the graphite susceptor to the growth temperature. The same precursor chemicals were used in both systems.

3.2 Optical in situ monitoring system

In situ monitoring system provides direct information about the growth process of the samples during growth. The use of the reflectance measurement is based on the interference of the light reflecting from the interfaces between different materials. When a layer with a complex refractive index $n_{c1} = n_1 + i\kappa_1$ grows on substrate with a complex refractive index $n_{cs} = n_s + i\kappa_s$, the incident light is reflected from the surface of the layer and from the interface of the materials if $n_{cs} \neq n_{c1}$. Furthermore,

these two light rays, having travelled different optical distances, interfere with each other. Thus, the overall reflectance is a periodical function of the layer thickness if absorption in the material is small and the layer thickness adequate. The oscillations are called Fabry-Perot oscillations, and they can be used to determine layer thickness d or the refractive index n from the reflectance curve. The maxima of the interference pattern appear

$$d = \frac{m\lambda}{2n}, \tag{3.1}$$

where m is an even integer and λ is the measurement wavelength. Correspondingly, the minima of the interference pattern appear

$$d' = \frac{(m + 1/2)\lambda}{2n}. \tag{3.2}$$

In Eqs. 3.1 and 3.2 the thickness of the layer d (d') can expressed as a product of the growth time and growth rate: $d = r_{\mathrm{g}}t$. The growth rate can be determined if n is known. Similarly, n can be determined if the growth rate is known. Because n is a function of the layer composition, the composition of a ternary alloy layer can be determined if the growth rate is known.

Absorption in the material causes damping of the oscillations of the reflectance curve. The effect of the absorption can be taken into account by the imaginary part when complex refractive index $n_{\mathrm{c}} = n + i\kappa$ is used. The value of κ can be determined from the Fabry-Perot oscillations by measuring the intensity ratio of two consecutive peaks I_1/I_0 and their time difference Δt. Intensities I_0 and I_1 are values from which the reflectance of the layer surface has been substracted. The imaginary part of the complex refractive index, κ, can be written as

$$\kappa = \frac{\lambda}{4\pi r_g \Delta t} \ln\left(\frac{I_0}{I_1}\right). \tag{3.3}$$

However, when thin layers, such as quantum wells, are grown, the thickness of each layer is too small for the whole period of a Fabry-Perot oscillation to appear and a rather different shape is seen in the reflectance curve. In order to see changes caused by such thin layers it is important to choose a suitable wavelength for in situ monitoring [9].

In this work, an optical in situ monitoring system attached to the CCS MOVPE system was used. Fig. 3.2 shows a schematic picture of the commercial normal incidence reflectance setup. The optical ports of the in situ reflectance setup are located on top of the reactor chamber. The input and output light signals are carried via optical fibers to the actual measurement unit. The light source is a halogen lamp. Wavelength of 635 nm was used to study the structures. As the susceptor rotates, the reflectance measurement is performed for a certain area of the substrate surface on every rotation and the reflectance signal is averaged over the area. This increases the accuracy of the method over a single point measurement.

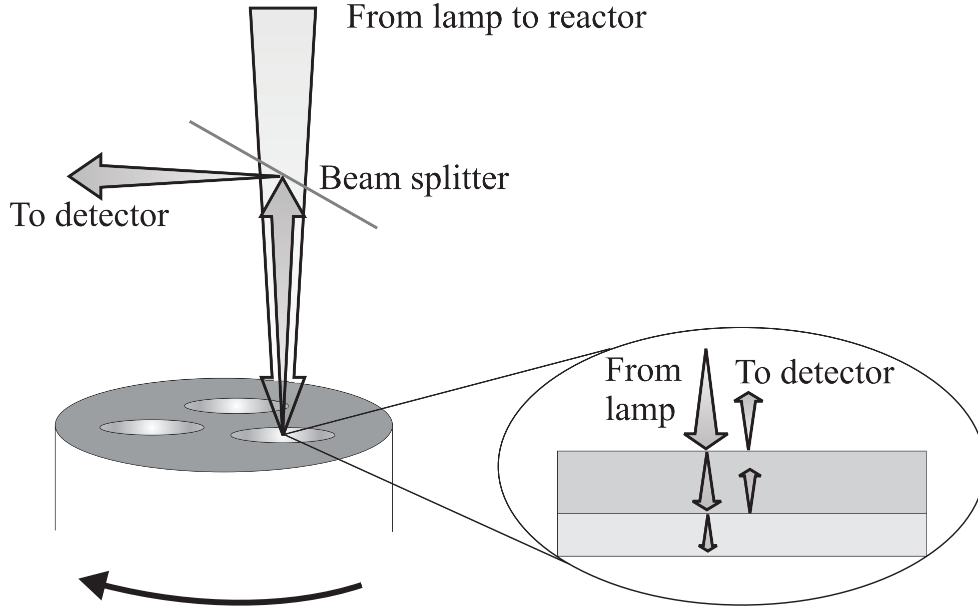

Figure 3.2: Schematic of the in situ reflectance measurement system.

3.3 X-ray diffractometry

X-ray diffraction (XRD) is a relatively fast and non-destructive method for characterisation of crystalline semiconductors. XRD characterisation is based on the diffraction of x-rays from the crystalline lattice planes. The angle θ between the diffracted beam and the diffracting lattice planes of the material can be described by the Bragg's law

$$2d \sin\theta = n\lambda \tag{3.4}$$

where d is the distance between two sequential lattice planes, n is an integer and λ is the x-ray wavelength. The lattice constant a_0 and d are related by equation $d = a_0(h^2 + k^2 + l^2)^{-1/2}$ where h, k and l are the Miller indices of the diffracting lattice plane. Assuming a near perfect crystal the lattice constant is a function of the composition of the layer and thus the composition of the sample can be determined from the diffraction pattern. The layer thicknesses can be determined from the fringes of the diffraction pattern.

A commercially available high-resolution x-ray diffraction (HR-XRD) apparatus was used to characterise the samples for this thesis. It has high accuracy when determining layer thicknesses of multilayer structures as well as binary and ternary alloy compositions. $\omega - 2\theta$ configuration was used in the measurements (ω is the angle between the incoming beam and the sample surface). If the offset angle between the lattice planes and the sample surface is zero, then $\omega = \theta$. However, usually there is a constant offset angle between ω and θ. The measured $\omega - 2\theta$ HR-XRD curves

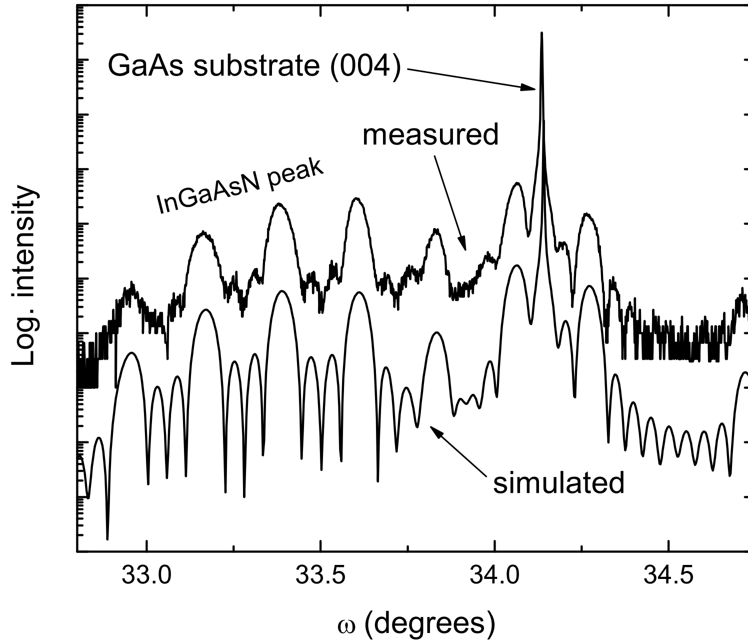

Figure 3.3: Typical result measured from a GaInNAs/GaAs MQW structure by HR-XRD (upper curve) and a simulation fitted to that (lower curve). The vertical offset between the curves is added for clarity.

were analysed with a simulation software.

Fig. 3.3 shows a typical HR-XRD curve from an InGaAsN/GaAs MQW structure. The simulated curve (lower curve in the figure) is used to determine the lattice constant of InGaAsN and the layer thicknesses. When characterising MQW structures consisting of one ternary and one binary alloy, *e.g.*, GaAsN/GaAs and InGaAs/GaAs, the composition determination by fitting is simple because of the relation between the ternary alloy lattice constant and the layer composition is unambiguous. For example, adding nitrogen into GaAs lattice decreases the lattice constant and thus the GaAsN (004) peak appears at a larger angle than the GaAs (004) peak. Similarly, when indium is added into GaAs, the lattice constant compared to GaAs increases and the (004) peak of InGaAs is at smaller angles compared to the GaAs (004) peak. However, if a quaternary alloy system, such as $In_xGa_{1-x}As_{1-y}N_y$, is studied with HR-XRD, the composition of the sample can not be directly calculated from the lattice constant acquired by the measurement, because there are two composition variables x and y affecting the lattice constant. Thus, x or y or their relation needs to be fixed in the fitting procedure. This can be

attained by employing a complementing measurement in addition to the HR-XRD. Nevertheless, the determination of the layer thicknesses using the HR-XRD curve is reliable also in the case of the quaternary layers because the determination of the thickness is independent of the layer composition.

3.4 Photoluminescence spectroscopy

The measurement of the optical properties of the samples is an important part of the research of III-V semiconductor structures in most of the cases. The main optical characterisation tool used in this study was photoluminescence (PL) spectroscopy, though also some reflectivity, absorption and time-resolved PL measurements were performed.

In PL measurements the sample is excited by laser irradiation. The photon energy of the exciting laser light has to be chosen so that it is capable to generate electron-hole pairs in the material, *i.e.*, the photon energy has to be larger than the bandgap. The excited carriers thermalise, diffuse and relax into energy levels near the band edges. Then, the electrons and holes may recombine spontaneously causing the material to luminesce isotropically. Transitions between the energy levels determine the spectrum of the luminescence. Thus, phenomena that influence the band structure of the semiconductors influence also the photoluminescence spectra. Such factors are, for example, temperature, composition and strain of the sample as well as the structure and quantum effects present in the sample. Additionally, signatures of doping or other impurity levels and excitons as well as defects can appear in the PL spectrum. Anyway, in direct bandgap alloy semiconductors the peak having the highest intensity is usually caused by recombination of carriers located near the band edges.

In the PL measurement system used in this work, a pump laser at 532 nm was used with various output powers. The laser beam was focused onto the sample with a set of mirrors and lenses. For low temperature measurements, the sample was placed into a cryostat and cooled down to the temperature of 10 K at minimum. Measurements at room temperature were also performed. The luminescence was collected from as large solid angle as possible in order to maximise the signal. The collected light was divided into its spectral components by a monochromator. Typically, a nitrogen cooled germanium detector was used after monochromator to measure the intensity of the spectral component. A computer was used to scan the selected wavelength area by controlling the grating of the monochromator. The computer was also used to record the measured intensities, *i.e.*, the spectrum of the luminescence.

4 MOVPE growth parameter optimisation for InGaAsN

This chapter discusses the MOVPE growth parameter optimisation for (In)GaAsN growth. The experimental aspects of the MOVPE technique were introduced in Section 3.1. Section 4.1 summarises the effect of growth and annealing temperatures on the nitrogen incorporation and Section 4.2 presents the effect of precursor flows on the nitrogen content. Section 4.3 outlines the importance of the choice of the carrier gas.

4.1 Growth and annealing temperatures

All the studied structures for this thesis were fabricated by MOVPE. The samples were MQW structures consisting of three or four (In)GaAs(N) QWs and GaAs barriers. The samples were not intentionally doped in any way. Semi-insulating epiready GaAs wafers with thickness of 350 μm were used as substrates in all the growth runs, except for the samples grown on germanium substrates for Publication VI.

The growth temperature is one of the first parameters to be optimised when dilute nitrides are grown. It has been found that lower growth temperatures than in typical III-V growth (over 600°C) have to be used to obtain significant nitrogen incorporation. Additionally, the overall trend is that the nitrogen content increases when the growth temperature decreases, *i.e.*, the nitrogen incorporation is temperature dependent. This is typical for dilute nitride growth regardless of the growth method used, see for example Ref. 73 and references therein. The optimal dilute nitride growth temperature considering both material quality and nitrogen incorporation was found to be 575°C (a thermocouple reading) for the CCS MOVPE and 570°C (also a thermocouple reading) for the horizontal reactor MOVPE.

The temperature set points used in the CCS system varied during the study. To fabricate the samples at the same temperature at all times, the imperfect decomposition of TMGa at the growth temperature was used for calibration. The decomposition of TMGa depends strongly on temperature at around 570°C [69]. Therefore, the growth temperature was adjusted so that the indium content of an InGaAs MQW

sample was always the same. This automatically leads to similar growth temperatures.

Annealing treatments were also performed in the MOVPE reactors. The annealing temperatures used in this study were 750°C and 700 °C for the CCS and horizontal reactors, respectively. The annealing time was always 10 minutes. During the annealing treatment, a sufficient TBAs flow was driven into the reactor in order to protect the topmost GaAs surface from arsenic desorption and consequent deterioration.

4.2 Precursor molar flows

In MOVPE growth the sample composition is determined by the ratios of the precursors in the reactor. In order to incorporate nitrogen into the InGaAs lattice very large DMHy/V molar flows ratios are required. However, nitrogen content of the samples in this thesis was found to be sensitive also to molar flow ratios which did not include DMHy. Additionally, it has been reported that the nitrogen incorporation efficiency depends also on the choice of precursors [71–73].

First, the nitrogen incorporation into GaAsN was studied. Fig. 4.1 shows the dependence of GaAsN nitrogen content on the TBAs/III molar flow. The nitrogen content is increasing with increasing TBAs/III molar flow ratio. The samples were grown at reactor pressures of 100 torr, 300 torr and 700 torr (approximately atmospheric pressure). The TMGa and DMHy flows to the reactor were identical for all the samples, which means that the DMHy/(TBAs+DMHy) molar flow ratio decreased with increasing TBAs flow and with increasing TBAs/III ratio. Thus, the nitrogen content of GaAsN is increased when the DMHy/V molar flow ratio is decreased. This result is discussed in publication I. A similar result has been achieved by Derluyn *et al.* at low pressure [74]. Their results show that the amount of TBAs in the reactor, in addition to the TBAs/III and DMHy/V ratios, is affecting the nitrogen incorporation. The nitrogen content of their samples increased with increasing TBAs flow and constant DMHy flow until an abrupt decrease was observed. In other words, in the nitrogen content vs. TBAs/III ratio there is a TBAs/III ratio where the nitrogen incorporation is at its maximum. At smaller TBAs/III ratios the nitrogen incorporation is increasing with increasing TBAs/III ratio and at larger TBAs/III ratios the nitrogen content of the sample decreases when the TBAs/III ratio is increased.

Our results as well as the results of Derluyn *et al.* could be caused by increased decomposition of DMHy precursor in TBAs rich atmosphere. However, Derluyn *et al.* suggest that the increase in nitrogen content when TBAs/III flow is increased is caused by surface related issues and that the reason of increased nitrogen content would be that the arsenic coverage of the surface promotes the adsorption of the

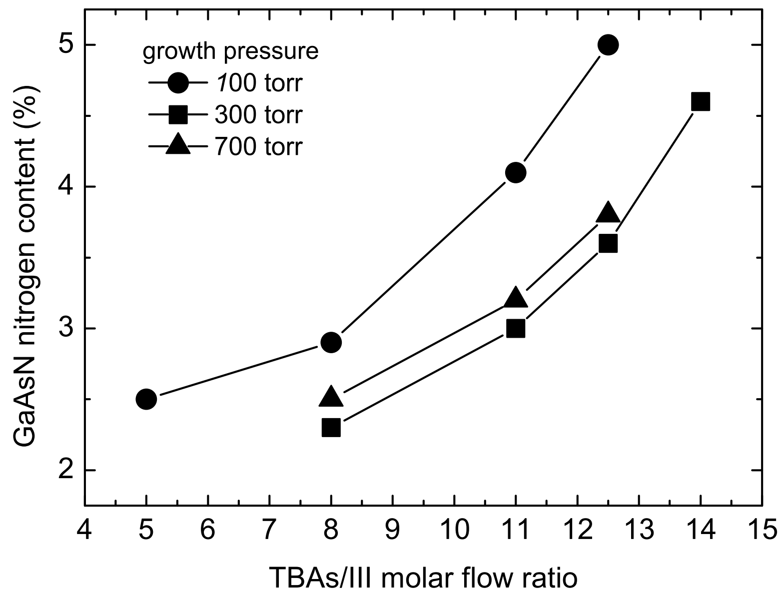

Figure 4.1: GaAsN nitrogen content as a function of the TBAs/III molar flow ratio used during the growth of the QWs. Samples grown at different pressures are denoted with different symbols.

DMHy molecules. When the arsenic coverage is too high the DMHy molecules are desorbed and the nitrogen content in the lattice starts to decrease. In addition to these results, Toivonen *et al.* observed a different behaviour of the nitrogen content when growing the samples at atmospheric pressure [53]. Their results indicate that the TBAs/III molar flow ratio should be minimised in order to obtain maximal nitrogen incorporation. The controversy of the results might be explained assuming that the samples of Toivonen *et al.* were grown in the TBAs/III range larger than the value of maximum nitrogen incorporation. In that case the results of Toivonen *et al.* are in agreement with our results as well as with the results of Derluyn *et al.*

The nitrogen incorporation into InGaAs was studied by changing the DMHy flow and keeping all the other flows as well as the growth temperature and pressure constant. Typically the dependence between the precursor flow and the sample concentration is straightforward. For example, at small indium contents the InGaAs indium content increases linearly as the TMIn molar flow is increased. However, the nitrogen content of InGaAsN is a superlinear function of the DMHy flow, which was clearly observed in publications II and III. Similar results have also been achieved by others [75].

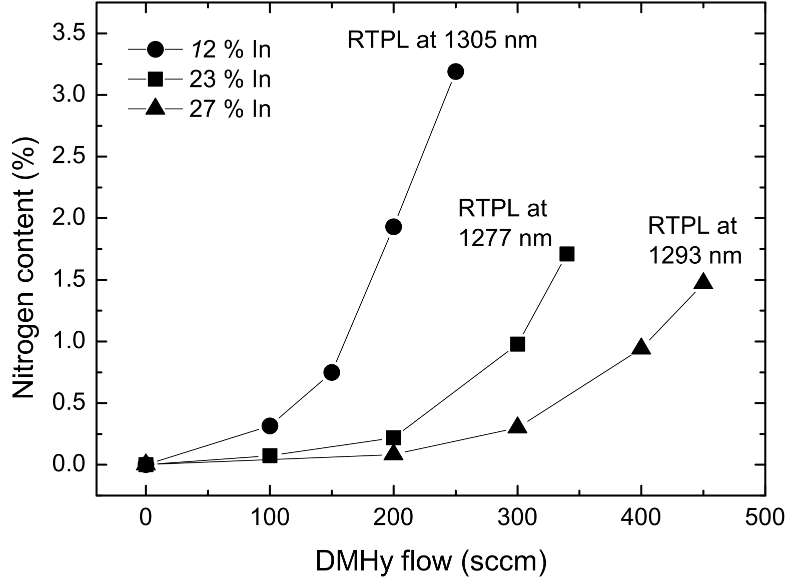

Figure 4.2: InGaAsN nitrogen content as a function of the DMHy flow. The DMHy/V molar flow ratio increased from 0 to 0.95 when DMHy flow range was 0-450 sccm.

Fig. 4.2 shows the InGaAsN nitrogen content as a function of the DMHy flow for samples containing 12, 23 and 27 % indium. The superlinear behaviour is observed for all the curves. The highest nitrogen contents at all DMHy flows were obtained from the samples with the lowest indium contents, *i.e.*, the nitrogen incorporation is less efficient with large indium contents. This has been previously reported, for example, by Bhat *et al.*, Friedman *et al.* and by Moto *et al.* [76–78].

There has been speculation about what might be the reason for the lower nitrogen incorporation efficiency when indium is present in the reactor. Some explanations do exist. Reactions between indium and nitrogen precursors have been more or less excluded, because lowered nitrogen incorporation has been reported in MOVPE reactors where the precursors mix just before the substrate and, therefore, prereactions are unlikely [78]. Additionally, the phenomenon has been observed also in MBE growth, where prereactions are not an issue [77]. It has been proposed that the weaker bonding of In-N compared to that of Ga-N might affect the nitrogen incorporation or that the surface segregation of indium during the growth of InGaAs reduces the nitrogen incorporation into the lattice [77]. Zhang and Zunger have suggested that nitrogen surface solubility to GaAs is enhanced compared to the bulk solubility, and that in the presence of indium adatoms the surface reconstruc-

tion is changed [79]. However, Suemune *et al.* have reported an enhanced nitrogen incorporation in the presence of indium in their MOMBE process [80].

Fig. 4.2 also shows the room temperature PL peak wavelengths for the most nitrogen rich samples in each series. The PL spectra were measured from as-grown samples. The same PL wavelength, approximately 1300 nm, can be achieved using several sample compositions, leading to fairly different characteristics of the material. For optically active components the indium content should be maximised in order to avoid the defects caused by nitrogen. However, *e.g.*, for mode locking SESAM structures a fast recovery time is required and, thus, larger nitrogen content is preferred.

4.3 Choice of carrier gas

The choice of the carrier gas is another factor which can be used to tune the nitrogen content of an (In)GaAsN sample. The typical choice for carrier gas in dilute nitride growth process is hydrogen (H_2) but the use of nitrogen gas (N_2) has also been reported [81, 82].

Fig. 4.3 shows results measured from two InGaAsN/GaAs MQW series, one grown in H_2 and the other in N_2. The InGaAsN nitrogen content is shown as a function of the DMHy molar flow and a similar threshold like behaviour to what is shown in Fig. 4.2 is found regardless of the choice of the carrier gas. The samples grown in H_2 and N_2 ambients had nominally the same growth parameters, expect for the carrier gas. However, the indium contents of the samples were 18 % and 14 % for samples grown in H_2 and N_2 ambients, respectively. The lower indium content of the samples grown in N_2 is considered to be caused by the lower thermal conductivity of the N_2 gas: because the heat is not transferred from the susceptor as efficiently as it is transferred in H_2 ambient, the susceptor and, therefore, the substrate surface remain at slightly higher temperature in N_2 ambient. As written previously, the TMGa precursor does not completely decompose in the dilute nitride growth temperatures. Thus, if the temperature in N_2 is higher, the fraction of the decomposed TMGa is higher, TMIn/TMGa molar flow ratio is lower and consequently the indium content of the sample is lower.

HR-XRD analysis showed that the growth rate in N_2 was decreased by 37 % compared to the growth rate in H_2. The growth rate decrease is supposed to be caused by the smaller diffusion coefficient of the metal-organics in N_2 gas [81]. The precursors are also decomposed differently in different atmospheres, which might influence the growth rates.

The possibility of the slightly higher surface temperature and the reduced growth rate observed when N_2 carrier gas was used probably affect the nitrogen incorpo-

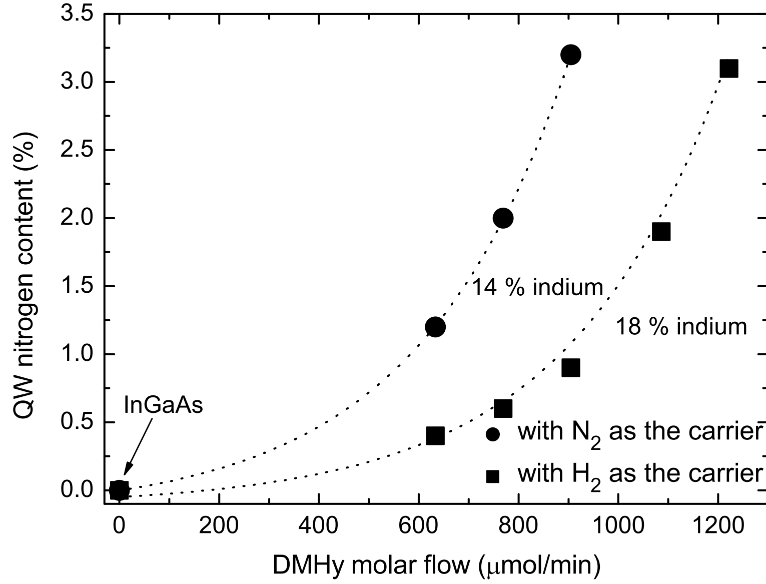

Figure 4.3: Effect of the carrier gas on the nitrogen incorporation into InGaAs.

ration, but they alone are not sufficient to explain it entirely. The threshold value of the nitrogen incorporation is lower when the samples are grown in N_2 and the difference in the nitrogen content increases as the DMHy molar flow is increased. In addition to the data shown in Fig. 4.3, a sample with a DMHy molar flow of 1100 μmol/min was grown in N_2. The sample was deteriorated and the nitrogen content could not be determined by HR-XRD analysis. If the curve in Fig. 4.3 for N_2 grown samples is followed, the sample grown with 1100 μmol/min would have a nitrogen content of approximately 6 % or even higher. Other groups have found a critical nitrogen content, above of which the material quality deteriorates rapidly [83, 84]. It is supposed that the critical nitrogen content in these growth conditions was exceeded which caused the sample deterioration. However, when growth was performed in H_2, DMHy flow of 1100 μmol/min leads to a nitrogen content of only 2 %. Based on these results the nitrogen incorporation into the QWs is more efficient when the structure is grown in N_2.

Effect of the choice of the carrier gas on hydrogen incorporation was also briefly studied. The unintentional and undesired incorporation of hydrogen into the InGaAsN lattice was found to be more efficient when H_2 was used as a carrier gas, as reported in Publication III. For both carrier gases the hydrogen incorporation to the InGaAsN QWs was much larger than to GaAs barriers. This is considered to be

caused by the strong nitrogen-hydrogen bond formed between the atoms. Hydrogen is not believed to be incorporated from the molecular carrier gas, H_2, but more likely from the atomic hydrogen cracked from the precursors. An overview of the hydrogen incorporation and its effects on the material were given in Section 2.3.

5 Calculation and simulation of reflectance curves

Chapter 5 describes the calculation method of the theoretical reflectance curves. Section 5.1 explains the theory of reflection from a multi layer stack with increasing layer thickness and Section 5.2 outlines the simulation of the measured reflectance data.

5.1 Theoretical calculation of in situ reflectance curve

The in situ reflectance measurement is based on the reflection of light from interfaces and the interference of the reflected light rays, as was explained briefly in Section 3.2. To calculate the reflectance curve for a multi layer stack a matrix method is used. Matrix method has been successfully used for example for ex situ layer thickness measurements by Tarof *et al.* [85]. A schematic picture of a multilayer stack and the direct reflections of the transmitted beam at each interface is shown at the right hand side of Fig. 5.1. Multiple reflections are neglected in the figure for clarity.

First, the case of two layers having different refractive indices will be considered. The left hand side of Fig. 5.1 shows the electric fields of the propagating beam above and below one interface. E_+ and E'_+ are the fields propagating forward in layers above and below the interface, respectively. Correspondingly, E_- is the backward propagating field in the upper layer and E'_- is the backward propagating field in the lower layer. E'_+ and E'_- are taken to be at a distance of l from the interface. The fields in the layers are related by an interface matrix M_i and a propagation matrix M_p by

$$\begin{bmatrix} E_+ \\ E_- \end{bmatrix} = M_i M_p \begin{bmatrix} E'_+ \\ E'_- \end{bmatrix}. \tag{5.1}$$

M_i describes the reflection and transmission at the interface and M_p describes the propagation of the fields in the layer. They can be written

$$M_i = \frac{1}{\tau} \begin{bmatrix} 1 & \rho \\ \rho & 1 \end{bmatrix} \quad \text{and} \quad M_p = \begin{bmatrix} e^{jkl} & 0 \\ 0 & e^{-jkl} \end{bmatrix}, \tag{5.2}$$

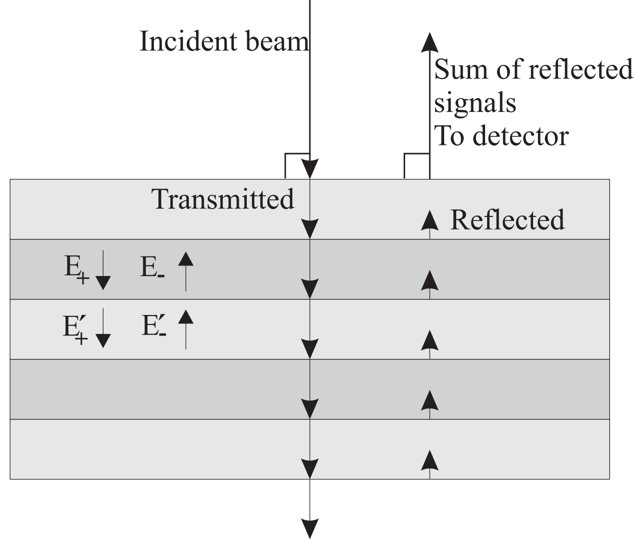

Figure 5.1: Schematic picture of a multi layer stack with two types of layers and the propagation of a light beam in it. Only the direct reflections are denoted in the figure, the rest are ignored for clarity. Also, fields E_+, E_-, E'_+ and E'_- propagating in two layers are denoted.

where $k = 2\pi n_c/\lambda_0$ and ρ and τ are the reflection and transmission coefficients, respectively, given by

$$\rho = \frac{n'_c - n_c}{n'_c + n_c}, \ \tau = \frac{2n'_c}{n'_c + n_c} \tag{5.3}$$

with n_c being the complex refractive index on the upper layer and n'_c the complex refractive index on the lower layer. The use of complex refractive indices is required because absorption in the materials cannot be neglected.

The forward and backward propagating electric fields in a structure with m interfaces can be obtained by using a product of all the M_i and M_p matrices over the whole structure, *i.e.*,

$$\begin{bmatrix} E_+ \\ E_- \end{bmatrix} = M_{i1} M_{p1} \cdots M_{p(m-1)} M_{im} \begin{bmatrix} E'_+ \\ 0 \end{bmatrix} \tag{5.4}$$

where $E'_- = 0$ because there is not any backward propagating field in the substrate.

The in situ reflectance monitoring system measures the intensity of reflected light as a function of time. The measured reflectance is simply the absolute value of the ratio of E_- and E_+ squared

$$R = \left| \frac{E_-}{E_+} \right|^2 . \tag{5.5}$$

Based on this matrix method a simulation algorithm was implemented. To get the

time evolution of the reflectance the thickness of the topmost layer was increased according to the growth rate. In the fitting procedure of the experimental data the least squares minimisation was utilised. The important parameters for fitting the measured data with the matrix method algorithm are the complex refractive index $n_c = n + i\kappa$ and the growth rate of each layer.

Fig. 5.2 shows the reflectance curve measured during growth of a GaAs on $Al_{0.89}$GaAs structure with thick GaAs and AlGaAs layers (315 nm and 270 nm, respectively). The growth temperatures of the layers were 690°C and 670°C for $Al_{0.89}$GaAs and GaAs, respectively. The difference of 20°C in the growth temperature does not change the value of reflectance significantly, as is shown in the figure (the temperature ramp is denoted). This two layer structure was grown on GaAs substrate, which causes difference in the complex refractive index between the substrate and the AlGaAs layer, and later there is a difference in the complex refractive indices between the epitaxial layers of AlGaAs and GaAs. Because of the different complex refractive indices and because the layers are thick enough, several complete Fabry-Perot oscillations are observed during growth of both layers. The measured curve is denoted with open circles and the fit calculated using the matrix method is shown with a solid line.

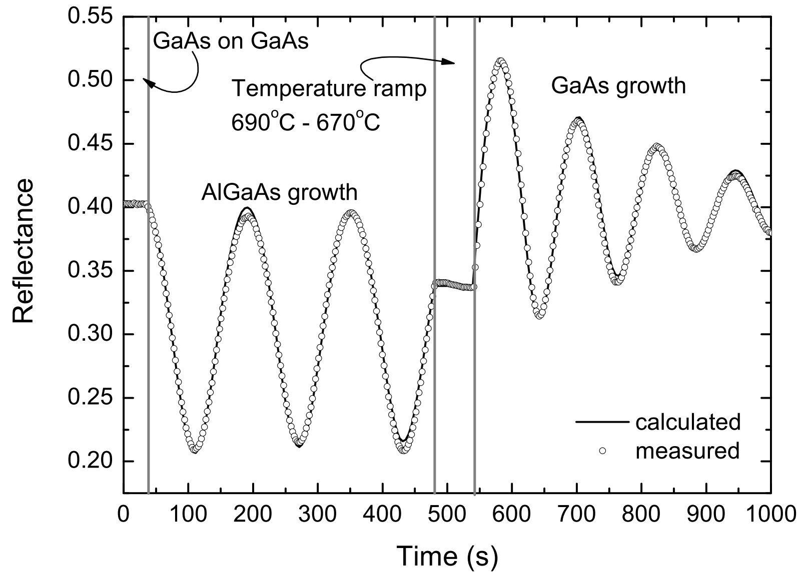

Figure 5.2: Reflectance curve measured during growth of GaAs on AlGaAs structure (open circles) and a theoretical reflectance curve (solid line). Several periods of Fabry-Perot oscillations occur during growth of both materials.

There is a very good agreement between the measured and calculated curves in Fig. 5.2. By fitting, complex refractive indices $3.3 - 0.03i$ and $4.2 - 0.3i$ were obtained for AlGaAs and GaAs, respectively. The values are in good agreement with the results reported previously by others [6, 86, 87]. The much stronger damping of the reflectance signal during growth of the GaAs layer in is caused by the larger imaginary part of $n_{\mathrm{c,GaAs}}$ compared to that of $Al_{0.89}GaAs$ at 635 nm.

5.2 Simulation of reflectance data

In situ reflectance measurement is sensitive to changes of the complex refractive index of the layers. However, in real life the changes which are observed in the in situ reflectance curve originate also from, *e.g.*, temperature changes and the native oxide removal process. Fig. 5.3 shows a complete reflectance curve measured during the growth process of a GaAsN/GaAs MQW structure. The curve shows the reflectance change with respect to the original reflectance level as a function of the growth time.

What is not shown in Fig. 5.3 is that the material quality during growth affects the reflectance level. For example, if the surface is considerably roughened during the growth process, the reflectance value decreases due to the scattering of light on the surface. In heteroepitaxial growth the changes at the interface, for example serious intermixing, can be observed. Similarly, with increasing material quality and consequently decreasing scattering the reflectance increases. However, if growth of high quality material identical to the substrate is grown directly on the substrate, changes in the reflectance do not occur. This is visible in Fig. 5.3 when the two GaAs buffers are grown (the first at 670°C and the second at 575°C, the growth regions are denoted in the figure). The reflectance value remains constant during GaAs on GaAs growth.

From Fig. 5.3 it is clearly seen that the growth temperature has a significant effect on the reflectance level. It is well known that the complex refractive index of a certain material is a function of temperature. Therefore, all the QW structures studied for this thesis were fabricated at approximately the same temperature. In addition, the growth temperature dependence of the complex refractive index of GaAs was studied by growing thick GaAs layers on AlGaAs layers at different temperatures (see Fig. 5.2 for an example). This was done also to get a reliable value for $n_{\mathrm{c,GaAs}}$ at the dilute nitride growth temperature for the matrix method simulations, because the use of previously reported room temperature values for the optical constants of (Al)GaAs [88] do not give accurate results at elevated temperatures. Values of $4.0 - 0.3i$, $4.1 - 0.3i$ and $4.2 - 0.3i$ were obtained for GaAs at growth temperatures of 575°C, 620°C and 670°C, respectively.

The growth region of a GaAsN/GaAs MQW structure is also denoted in Fig. 5.3.

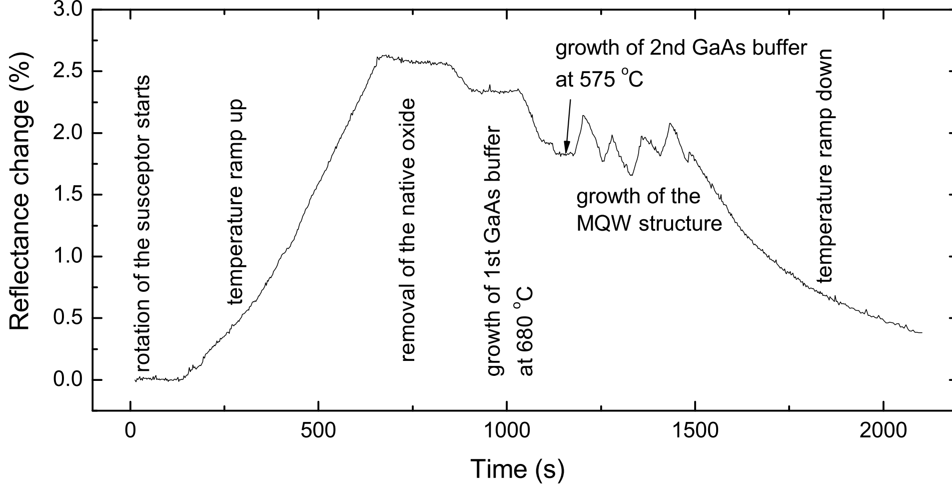

Figure 5.3: Reflectance curve measured during a process run of a GaAsN/GaAs MQW structure. Different origins of the reflectance changes are denoted in the figure.

A reflectance curve shape typical for a thin layer structure can be observed. In the reflectance curve measured during growth of the MQW structure the complete Fabry-Perot oscillations are not observed. Instead, the reflectance curve of the MQW structure consists of several sections with more or less linear change in reflectance as the material being grown is changed. This absence of the complete Fabry-Perot oscillations means that Eqs. 3.1, 3.2 and 3.3 can not be applied to extract n and κ of the layers in a MQW structure. However, this thesis presents a study of the use of fitting the theoretical reflectance curves calculated by the matrix method to analyse the reflectance curves of thin layer structures. It was observed that the method is applicable for dilute nitride MQW in situ analysis.

When calculating the theoretical reflectance curve for the fitting process, the complex refractive index and the growth rate of each layer in the structure are needed. All these parameters can be free in the fitting process. However, to obtain reliable data from the QW material the number of free parameters was reduced. First of all, the complex refractive index of the GaAs barriers, $n_{\mathrm{c,GaAs}}$, was fixed to $4.0 - 0.3i$. The value was obtained during growth of the GaAs on AlGaAs bulk layer structure grown at 575°C. Additionally, the growth rates of the layers were fixed to correspond to the layer thicknesses obtained by XRD measurements. Naturally, growth rate is an individual parameter for each sample. Thus, after fixing the value of $n_{\mathrm{c,GaAs}}$ and

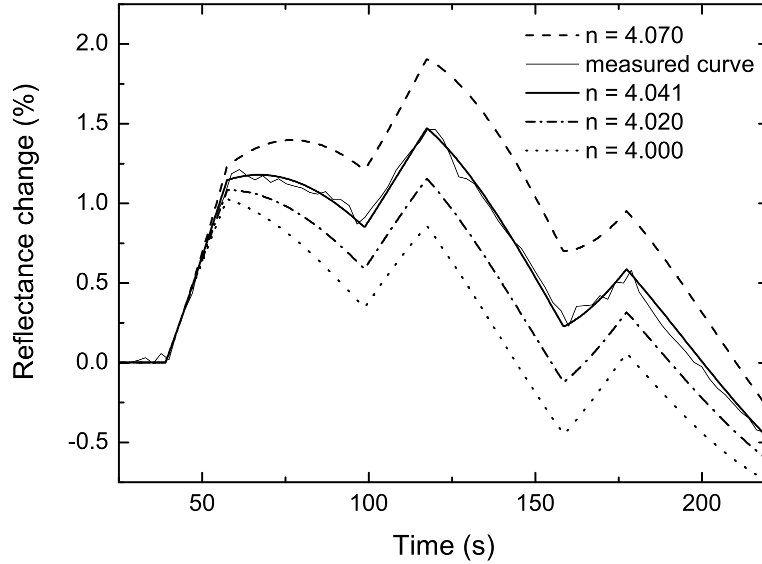

Figure 5.4: Theoretical reflectance curves calculated with different values of n and with a constant $\kappa = -0.374$. The experimental curve is measured during an InGaAs/GaAs MQW structure growth.

the growth rates of the layers in the fitting procedure, the only parameter adjusted in the fitting was the complex refractive index of the QW material. In other words, the result of the fitting process is $n_{\mathrm{c,QW}} = n_{\mathrm{QW}} + i\kappa_{\mathrm{QW}}$. Finally, to compensate the vertical offset between the measured data and the theoretical one, the calculated reflectance was adjusted to the GaAs buffer reflectance level.

To demonstrate the sensitivity of the method and to distinguish the effects of n and κ on the reflectance curves of thin layer structures, curves were calculated by keeping the other one fixed and changing the other. Fig. 5.4 shows several calculated reflectance curves and one experimental curve for an InGaAs/GaAs triple QW structure. The reflectance curve is given with respect to the GaAs buffer layer reflectance value. The indium content of the QWs was 19 %. The calculated curves have been obtained by changing the value of n from 4.000 to 4.070 and the value of κ has been fixed to -0.374. The best fit was found with a value of $n = 4.041$. Fig. 5.5 shows the same experimental curve and several calculated reflectance curves in which the value of κ has been changed between -0.325 and -0.400 and n has been fixed to 4.041. The best fit was obtained with a value of $\kappa = -0.374$. Thus, by simulation the best fit is obtained using a complex refractive index of $n_{\mathrm{c}} = 4.041 - 0.374i$.

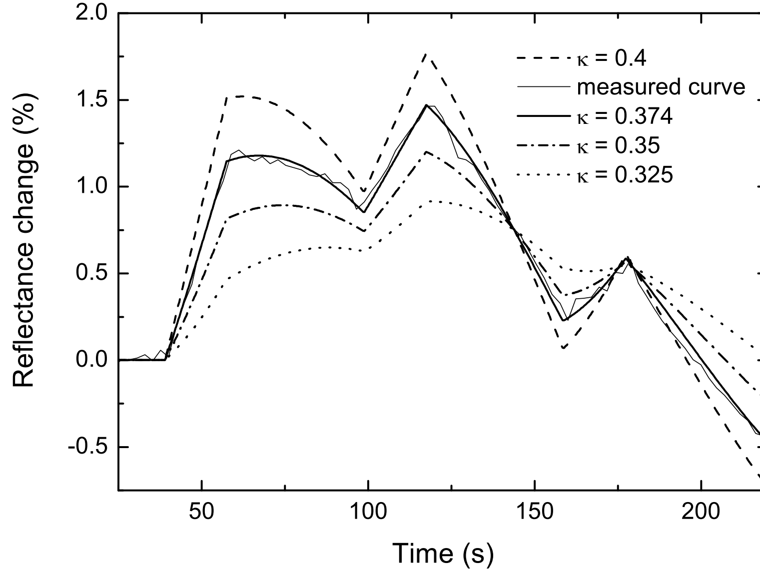

Figure 5.5: Theoretical reflectance curves calculated with different values of κ and with a constant $n = 4.041$. The experimental curve is measured during an InGaAs/GaAs MQW structure growth.

Figs. 5.4 and 5.5 illustrate the effects which the real and imaginary parts of the complex refractive index have to the shape of the reflectance curve. n and κ tend to change the reflectance curve differently. n influences the overall reflectance level of the curve whereas κ causes mainly a change in the slope of the curve obtained during growth of the QWs. Thus, as the changes in n and κ have so different consequences on the shape of the reflectance curve, they can be determined more or less independently from the in situ data.

The complete Fabry-Perot oscillations do not occur during growth of three or four QWs with typical barriers because the layers are too thin. However, the Fabry-Perot oscillations are present in the shape of those reflectance curves as well. Fig. 5.6 shows the measured and calculated reflectance curves for a stack of 20 InGaAsN/GaAs QWs. Additionally, a curve calculated using the effective complex refractive index of the QW stack, *i.e.*, thickness weighted average of the complex refractive indices of InGaAsN and GaAs, is shown in the figure. The value of $n_{\mathrm{c,eff}}$ was 4.010-0.353i. The growth rate of the virtual layer was also a weighted average of the growth rates of the barriers and QWs and had a value of 0.303 nm/s. Thus, the curve would appear if a bulk layer with $n_{\mathrm{c,eff}} = 4.010 - 0.353i$ would be grown with the growth rate of 0.303 nm/s. This curve is called the average bulk curve.

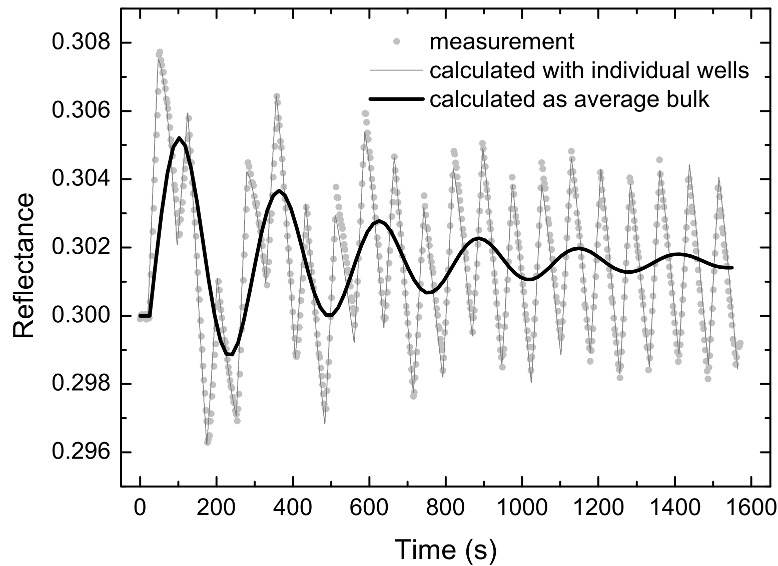

Figure 5.6: In situ curve measured during growth of a stack of 20 In-GaAsN/GaAs QWs, and a matrix method simulation fitted to that. The corresponding average bulk curve is shown with a thick black line.

Fig. 5.6 shows that the measured reflectance curve is very well in agreement with the simulation curve calculated with QWs and barriers. However, it is also seen that the shape of the average bulk curve is present in the reflectance curve measured during growth of QW structures. Thus, the Fabry-Perot oscillations are part of the reflectance curves of thin layer structures even though whole oscillations during the growth of single material can not be observed.

6 Determination of dilute nitride QW composition and quality by optical in situ monitoring

This chapter describes the main results obtained by in situ reflectance measurements on QW structures. Section 6.1 introduces a straight forward method to determine the QW composition. We call this technique the slope method. In Section 6.2 the in situ reflectance data is compared with theoretically calculated reflectance curves, which allows us to study the whole MQW structure. Finally, Section 6.3 discusses observations made on the quality of the structures during growth.

6.1 Slope method

As shown in Chapter 5, changes in the in situ reflectance curve occur during the growth of layers having different complex refractive indices. When the layer thicknesses are small compared to the wavelength, complete Fabry-Perot oscillations do not appear but the reflectance curve is composed of short sections of changing reflectance. During growth of each QW and barrier layer, the reflectance change can be approximated as a linear function of time, because each section represents only a very small fraction of a complete Fabry-Perot oscillation period. Here, the method which utilises this linearity in the QW composition determination process is called the slope method. The slope method and its use in practice are discussed in Publications I, II and III. The slope method can be used to analyse, *e.g.*, layer composition based on purely experimental data.

Fig. 6.1 shows the in situ reflectance curve measured during the growth process of an InGaAsN/GaAs MQW structure as a function of the growth time. The typical shape of the in situ reflectance curve of a MQW structure of this material combination is shown: the reflectance signal is increasing during QW growth and decreasing during barrier growth.

Parameters which are important for the use of the slope method are the reflectance change during growth of the QW, ΔR, and the growth time of the QW, Δt. Their ratio, the slope $\Delta R/\Delta t$ is shown in Fig. 6.1 as a solid line on the first QW. ΔR

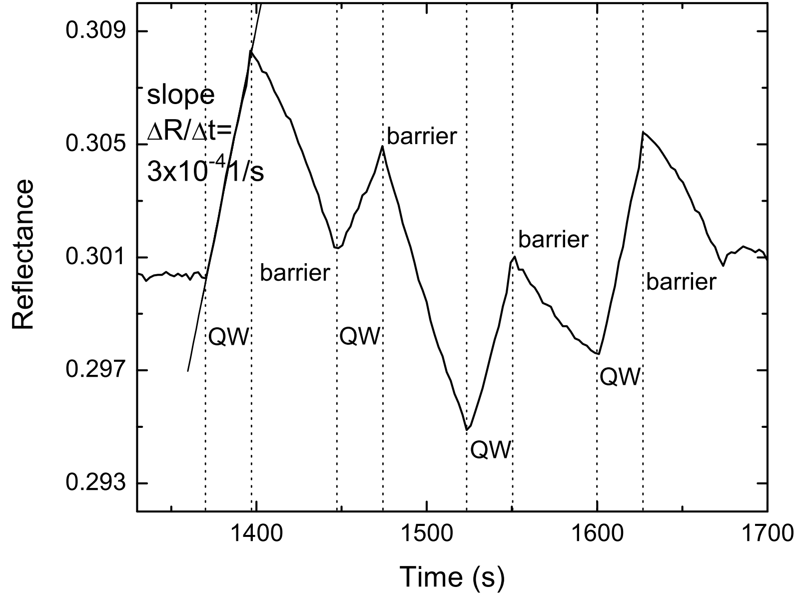

Figure 6.1: In situ reflectance curve measured during MOVPE growth of an InGaAsN/GaAs MQW structure. Linear fit to curve during growth of the first QW is also shown.

increases when the complex refractive index difference between InGaAsN and GaAs increases.

The rest of the results and discussion of the slope method in this section considers only the first QW of the MQW structure. The first QW is chosen to be studied in detail because of simplicity: when the first QW is grown, it is grown directly and only on GaAs. This means that there is only two interfaces for the incident light to reflect from, the atmosphere-QW interface and the QW-GaAs interface. If the other layers of the structure are under study, also all the interfaces between the QW and barrier layers already grown need to be considered.

In order to compare samples which have different growth rates, a growth rate correction is made to the slope $\Delta R/\Delta t$. The growth rate correction means that the slope $\Delta R/\Delta t$ is divided by the growth rate r_g of each layer. Then the growth rate corrected slope becomes $k = \Delta R/\Delta t \cdot 1/r_g = \Delta R/\Delta t \cdot \Delta t/\Delta d = \Delta R/\Delta d$, where Δt and Δd are the growth time and thickness of the layer. It should be noted that in order to make the growth rate correction effective, the real growth rate r_g has to be used in the correction. In this study r_g was obtained from the layer thicknesses

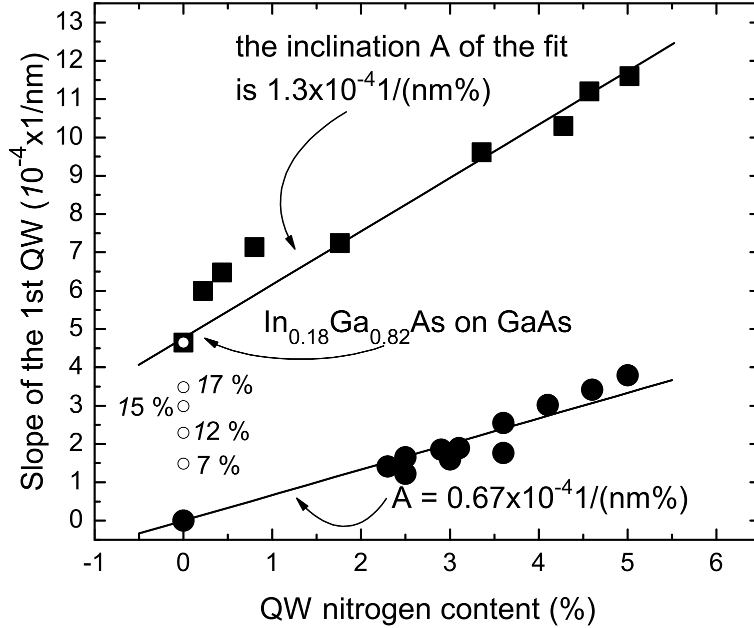

Figure 6.2: Growth rate corrected slopes k of the first QWs as a function of the QW nitrogen content for GaAsN, $In_{0.18}GaAsN$ and InGaAs. Linear fits forced via the [N]=0 data points are also shown for GaAsN and $In_{0.18}GaAsN$.

determined by the HR-XRD analysis.

The growth rate corrected slopes $k = \Delta R/\Delta d$ of the first QWs for samples with different compositions are shown in Fig. 6.2. Data points for GaAsN and $In_{0.18}GaAsN$ are shown as a function of the nitrogen content and additionally some InGaAs data points are also shown. The slope k of the first QW increases with increasing nitrogen and indium contents.

Fig. 6.2 shows also linear fits to the values of k for GaAsN and InGaAsN series as a function of the nitrogen content. The inclination $A = \Delta R/(\Delta d \cdot \Delta[N]) = k/\Delta[N]$ is different for indium contents 0 and 18 % as the values of $A = 0.0067$ nm^{-1} and $A = 0.013$ nm^{-1} were obtained for GaAsN and $In_{0.18}GaAsN$, respectively.

The value of A is constant over this nitrogen content range but it changes as a function of the indium content and needs to be determined experimentally for each indium content. This means that both indium and nitrogen content can not be determined simultaneously by the slope method. However, when the indium content

and the value of A are known, the nitrogen content of the sample can be determined using the equation

$$[N] = \frac{k_{InGaAsN} - k_{InGaAs}}{A}, \tag{6.1}$$

where k_i is the growth rate corrected reflectance slope $\Delta R/\Delta d$ for material i. Naturally, Eq. 6.1 holds also for GaAsN when the indium content is taken to be zero and $k_{\mathrm{GaAs}} = 0$.

The same method was used to study the InGaAs/GaAs QW samples with various indium contents. Linear dependence with $A = 0.0022$ nm^{-1} was obtained as a function of the indium content (fitted to data points in the indium content range 0-19 %, figure not shown here). The value of k_{InGaAs} or the indium content (when the other one is known) can be obtained using the Eq. 6.1 as it can be used for GaAsN and GaAs.

The value of A for InGaAs was observed to be smaller than that for GaAsN. Additionally, A for InGaAs was much smaller than A for InGaAsN for changing nitrogen content. Thus, a conclusion can be made that the effect of nitrogen on k is larger than the effect of indium, and also that the influence of nitrogen seems to be increased in more indium rich material.

The accuracy of the method is rather good, when the first QW of the structure is considered. Typical deviation from the linear fit in the nitrogen content of GaAsN, for example, is less than 0.5 %-units. The slopes of the barriers and the other QWs can also be determined from the reflectance curve. However, the field of application of the slope method is more or less limited to the study of the first QW because clearly the study of the other layers is more complicated and the accuracy of the method is not as high. Fig. 6.1 shows that the reflectance curves measured during the QW and barrier growth are actually not linear. Especially clear it is for the barriers, which all show nonlinear tendencies. For these reasons it is favourable to use another method for the analysis of the complete MQW structure.

6.2 Experimental data and matrix method

Matrix method can be used to calculate the reflectance curve utilising the interface and propagation matrices. The calculation was introduced in Section 5.1. In this section the matrix method is used to analyse the measured in situ reflectance data by comparing measured and calculated reflectance curves. As a result of the fitting process, values for the complex refractive indices of the materials can be obtained. The real and imaginary parts of the complex refractive index of (In)GaAs(N) are related directly to the alloy composition, as will be shown.

For all the results and discussion of this section, the growth rates of all the layers

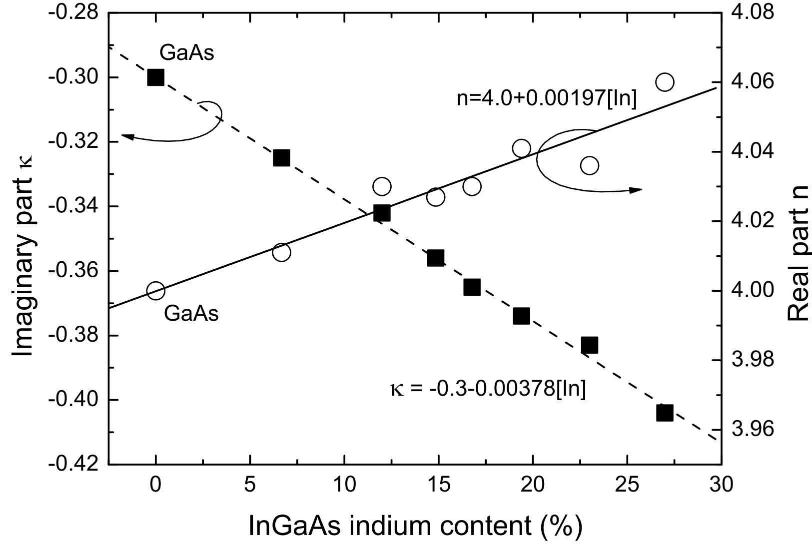

Figure 6.3: Real and imaginary parts of the complex refractive index of InGaAs as a function of the indium content. Linear dependencies are illustrated with linear fits to both parts. The linear fits are forced via the GaAs data points.

were determined via HR-XRD measurements and simulations and the growth rate was not adjusted during the fitting procedure. Additionally, $n_{\mathrm{c,GaAs}} = 4.0 - 0.3i$ was obtained from the bulk layer growth at 575°C and it was kept constant during all fitting steps. When doing so, the number of free parameters was reduced to only $n_{\mathrm{c}} = n + i\kappa$ of the QW material.

First, InGaAs/GaAs triple QW structures were studied. Fig. 6.3 shows the real and imaginary parts, n_{InGaAs} and κ_{InGaAs}, of the complex refractive index of InGaAs as a function of the indium content. The indium content range of 0-27 % was studied. Both n and κ change as the indium content is changed and they show a clear linear tendency. The linear fits shown in Fig. 6.3 were forced via the GaAs points.

From the linear fit, the real part of the complex refractive index of InGaAs can be written as

$$n_{InGaAs} = n_{GaAs} + B_{n,InGaAs} \cdot [In] \tag{6.2}$$

where $B_{\mathrm{n,InGaAs}}$ is the slope of the linear fit and has a value of 0.197. If the value of n_{InGaAs} is assumed to follow the linear approximation between the values n_{InAs} and n_{GaAs}, we get $B_{\mathrm{InGaAs}} = n_{\mathrm{InAs}} - n_{\mathrm{GaAs}}$. Baek *et al.* have reported a value 4.255 for n_{InAs} at 535°C at the detection wavelength of 632.8 nm [7], which would

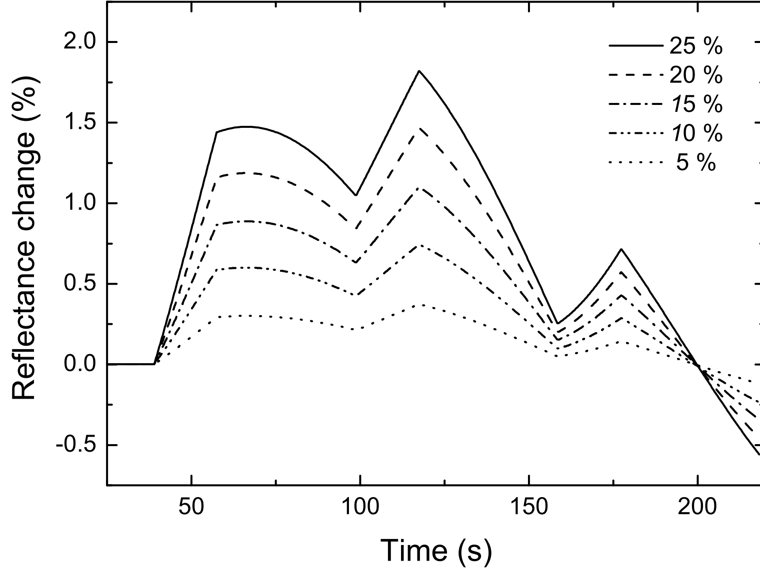

Figure 6.4: Calculated reflectance curves for InGaAs/GaAs triple QW structures with different indium contents. The calculations have been performed using n_{InGaAs} and κ_{InGaAs} obtained by Eqs. 6.2 and 6.3.

lead to $B_{\mathrm{InGaAs}} = 0.255$. The difference to the value measured here is probably due to difference in temperature and the possible nonlinear behaviour of n. For the imaginary part of the complex refractive index of InGaAs, κ_{InGaAs},

$$\kappa_{InGaAs} = \kappa_{GaAs} + B_{\kappa,InGaAs} \cdot [In] \tag{6.3}$$

where $B_{\kappa,\mathrm{InGaAs}}$ is the slope of the linear fit, which has a value of -0.373.

The indium content of InGaAs can be determined from Eqs. 6.2 and 6.3 by measuring either n_{InGaAs} or κ_{InGaAs} or both when the constants B_{InGaAs} are known. However, it can be observed that $B_{\kappa,\mathrm{InGaAs}} > B_{\mathrm{n,InGaAs}}$, which indicates that κ_{InGaAs} is more sensitive to changes of the indium content than n_{InGaAs}. Because of that, the accuracy of the determination does not increase if both parts are utilised and, thus, in the case of InGaAs ternary alloy system the imaginary part is recommended over the real part for composition determination. Also, as Fig. 6.3 shows, the scattering of the data points is larger for the real part and, therefore, using n_{InGaAs} causes larger error to the indium content determined *in situ*.

Fig. 6.4 shows calculated reflectance curves of InGaAs/GaAs triple QW structures with various indium contents. In the calculations, n_{InGaAs} and κ_{InGaAs} have been

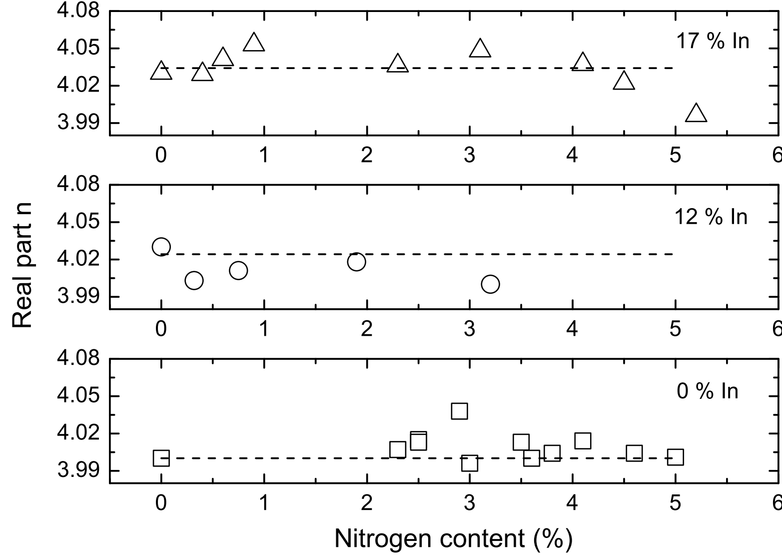

Figure 6.5: Real part of InGaAsN complex refractive index as a function of the nitrogen content for several indium contents.

obtained using Eqs. 6.2 and 6.3 for each indium content. The effect of the increasing indium content is clearly seen in the figure. From this figure also the power of the physical matrix method over the experimental slope method becomes clear: when the growth rates of the layers and the constants B_i are known, the reflectance curve of the whole structure with a certain indium content can be calculated with the matrix method. An important advantage is also that all the QWs in the MQW structure can be analysed separately, *i.e.*, the composition variations between different QWs can be observed. However, such a work was not included in this study.

Next, the reflectance curves measured during growth of (In)GaAsN MQW samples were studied. Fig. 6.5 shows the real part of the complex refractive index of InGaAsN as a function of the nitrogen content for several indium contents. The value of n_{InGaAsN} scatters around the value of n_{InGaAs} for all the investigated indium contents. The trend for all the series is that the real part of the refractive index of InGaAsN does not change as a function of the nitrogen content, *i.e.*,

$$n_{InGaAsN} = n_{InGaAs}. \tag{6.4}$$

This is noteworthy because clear linear increasing tendency was obtained for InGaAs with increasing indium content and because low nitrogen concentration is known to change several other properties of (In)GaAsN.

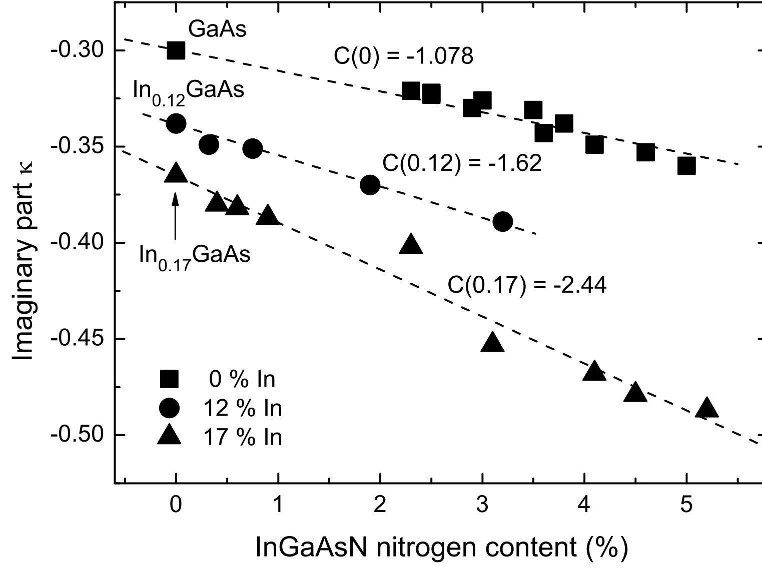

Figure 6.6: Imaginary part of InGaAsN complex refractive index as a function of the nitrogen content for several indium contents.

To complete the study of $n_{\mathrm{c,InGaAsN}}$, Fig. 6.6 shows the imaginary part of the complex refractive index of InGaAsN as a function of the nitrogen content for several indium contents. A clear dependence of $\kappa_{\mathrm{InGaAsN}}$ on the nitrogen content is seen for all the indium contents studied. Furthermore, the dependency seems to be linear, as was found earlier for κ_{InGaAs}. The linear fits to the data points are shown in the figure. The imaginary part of the complex refractive index of InGaAsN $\kappa_{\mathrm{InGaAsN}}$ can be written as

$$\kappa_{InGaAsN} = \kappa_{InGaAs} + C([In]) \cdot [N] \qquad (6.5)$$

where κ_{InGaAs} is the value of κ without nitrogen and $C([In])$ is the indium content dependent slope of the linear fit. The value of C in Eq. 6.5 is indeed dependent on the indium content of the material, as is shown in Fig. 6.6. Based on the values of $C([In])$ obtained with the indium contents 0 %, 12 % and 17 % it can be perceived that the indium content dependence of $C([In])$ is nonlinear. However, the linear dependence of $\kappa_{\mathrm{InGaAsN}}$ on the nitrogen content of the material is rather important for the in situ characterisation of QWs of this quaternary alloy.

When studying the complete composition of InGaAsN *in situ*, n_{InGaAsN} can be used to determine the indium content because n_{InGaAsN} does not depend on the nitrogen content. Moreover, $n_{\mathrm{InGaAsN}} = n_{\mathrm{InGaAs}}$ is linearly dependent on the indium content of the sample. After the indium content is known from the real part Eq. 6.5 can

be used with the valid $C([In])$ for the determination of the QW nitrogen content. Thus, the complex refractive index measured during the growth process can be used to determine the composition of the total composition of the quaternary alloy InGaAsN QWs.

The accuracy of the determination of the total composition of InGaAsN QWs is complicated to estimate. Because of its nature, n is more sensitive to all sorts of unidealities appearing during growth and measurement: the overall level of the reflectance signal can change for many reasons. In addition, the accurate determination of n usually requires a growth of a MQW structure, whereas the value of κ can be quite accurately determined during growth of a single QW. Furthermore, the value $B_{\mathrm{n,InGaAs}}$ is over ten times smaller than for example $C(0.17)$ indicating a much weaker dependence on the composition and, thus, lower sensitivity to the indium content. However, both parts of $n_{\mathrm{c,InGaAsN}}$ are needed in composition determination of an InGaAsN MQW sample. Moreover, the indium composition using n_{InGaAsN} needs to be determined first in order to obtain the nitrogen content. Thus, inaccuracy in the determination of the indium content is straightforwardly transferred into $C([In])$ and into the determination of the nitrogen content. As a result, to make the measurement and the determination process of the composition more reliable it would be favourable that the sensitivity of n to unidealities would be decreased. For example, the intensity of the light source could be kept constant more accurately using a feedback from the measurement of the source intensity. In addition, more work is required to explore the indium content dependence of the constant $C([In])$ in Eq. 6.5.

Another issue which requires a thorough study is the determination of the growth rate during growth of thin layer structures. At the moment, the determination of the growth rates of the layers need ex situ measurements. However, for ternary alloys the determination of the growth rate and the composition might be possible, if the relation between n and κ is known. For InGaAs, the relation can be obtained through Eqs. 6.2 and 6.3, *i.e.*,

$$n_{InGaAs} = n_{GaAs} + \frac{B_{n,InGaAs}(\kappa_{InGaAs} - \kappa_{GaAs})}{B_{\kappa,InGaAs}}. \tag{6.6}$$

The preliminary fits to the experimental InGaAs MQW data show that a decent fit can be found. This would be a significant advantage for the in situ monitoring of the MQW structures fabricated from InGaAs material system. Anyway, the growth rate of the GaAs barrier layers can be determined *in situ*, because n_{c} for GaAs is known.

6.3 Observing layer quality during growth

The in situ reflectance curve can also be used to estimate material quality during growth. The quality analysis performed by in situ reflectance monitoring is qualitative but still sometimes provides necessary information about the structure.

Dilute nitride studies often consider maximising the nitrogen content. However, it is quite well known that beyond a certain nitrogen composition, the material quality might decrease drastically [83, 84]. Fig. 6.7 shows reflectance curves measured during growth of a high quality (6.7a) and poor quality (6.7b) GaAsN/GaAs MQW structures. Deterioration of the structure in 6.7b is caused by exceeding the critical nitrogen content. The deterioration of the structure can occur during growth of other material systems, for example, when the critical thickness of a layer is exceeded and similarly it shows in the in situ reflectance curve. By monitoring growth *in situ*, the deterioration can be observed immediately when it occurs.

There are two major issues, which separate Figs. 6.7a and b from each other and illustrate the difference between the reflectance curves of the high quality and poor quality MQW structures. First, the overall reflectance level stays approximately the same during growth of the whole structure in the high quality sample (Fig. 6.7a). However, the overall level of the reflectance continuously decreases as the number of

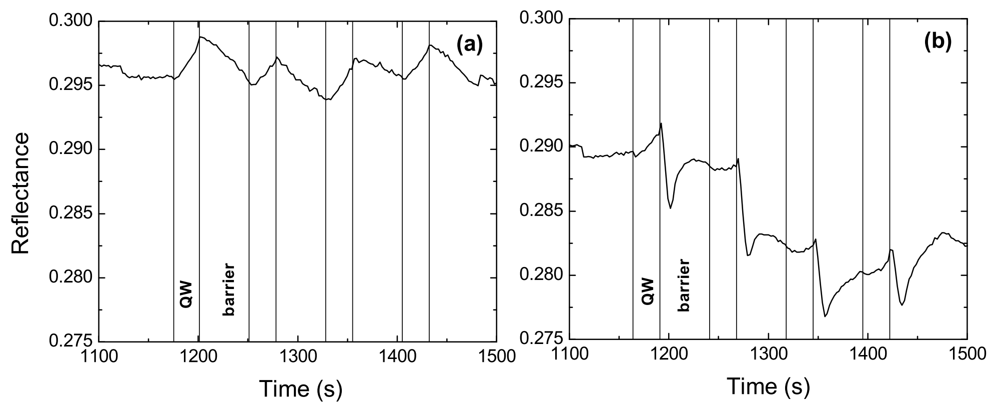

Figure 6.7: Reflectance curve measured during growth of a high quality sample (a) and a poor quality sample (b). The difference in the starting level of the reflectance is due to the lack of normalising the signal when these samples were grown and does not affect the result.

QWs is increased in the reflectance curve measured from the poor material quality sample (Fig. 6.7b). This alone indicates that the surface of the material is getting rough and thus scatters more light.

Secondly, because the layer thicknesses are so small that complete Fabry-Perot oscillations do not appear, the changes in the reflectance should be approximately linearly increasing (during growth of the QWs) or decreasing (during growth of the barriers). This, however, is true only for the high quality sample. For the sample with low material quality, a linear behaviour of the reflectance can only be observed during growth of the first QW. In the beginning of growth of each barrier, *i.e.*, at the point where DMHy flow to the reactor is switched off, a drastic drop of the reflectance is observed. After the drop, a recovery of the reflectance is observed during the barrier growth indicating that the quality of the surface is improving as the GaAs barrier is grown.

Deterioration of (M)QW structure can occur during growth for any material system for several reasons. Fig. 6.7 indicates that in this case the overlarge nitrogen content in the GaAsN layers hinders the growth process of the layers. These observations of the deterioration of the structure can not be made with any direct method after growth and the in situ reflectance curve provides valuable information when the reason of the deterioration is studied. Therefore, it is crucial to observe the growth process also from structure quality point of view.

7 Summary

Dilute nitrides are III-V semiconductors, which contain a low concentration of nitrogen. GaAs based dilute nitrides GaAsN and InGaAsN can be used in applications operating at optical communications wavelengths 1300 nm and 1550 nm due to the strong reduction of the bandgap introduced by nitrogen. However, to date their use in active devices has been limited by the defects caused by nitrogen.

In this thesis, metal organic vapour phase epitaxy (MOVPE) was used to grow (In)GaAs(N)/GaAs multi quantum well (MQW) samples. The growth process was monitored with a normal incidence reflectance setup at the wavelength of 635 nm. Ex situ sample characterisation was performed with high resolution x-ray diffraction (HR-XRD) and photoluminescence (PL) measurements.

Several MOVPE growth parameters were found to affect the nitrogen content of (In)GaAsN samples. The nitrogen content of GaAsN QWs was found to increase with increasing TBAs/III molar flow ratio when DMHy molar flow was kept constant. The nitrogen content of InGaAsN samples increased with increasing DMHy molar flow when all the other flows remained constant. In addition, the effect of the carrier gas was studied by changing the hydrogen carrier gas (H_2) to nitrogen carrier gas (N_2). The growth rate and indium content of the samples grown in N_2 were observed to be lower and the nitrogen content higher. The unintentional incorporation of hydrogen was also studied. An increased hydrogen concentration was observed in the nitrogen containing QWs compared to the barrier layers in all the samples. Additionally, the hydrogen concentration was higher in the samples grown in H_2 ambient.

In situ reflectance curves with complete Fabry-Perot oscillations were used to determine the complex refractive index of bulk GaAs at the growth temperature. Complete Fabry-Perot oscillations were not observed in the reflectance curves when MQW structures were grown due to the small thickness of the layers. The reflectance curves consisted of several approximately linear parts with sharp changes at the material interfaces.

The reflectance curves measured during the growth process of the MQW structures were found to be different for different sample compositions. First, a truly experimental method for determination of the QW composition was developed. The

method utilises the relation between the sample composition and the reflectance slope obtained during growth of the first QW of the MQW structure. Therefore, it was called the slope method. A growth rate correction was needed to compare samples with different growth rates. The slope of the first QW was found to increase linearly when the indium and nitrogen contents of InGaAs and GaAsN, respectively, increased. The slope of the quaternary alloy InGaAsN was affected by both nitrogen and indium contents and, therefore, both cannot be determined simultaneously *in situ* with this method. Additionally, the slope method is more or less limited to the composition determination of the first QW.

Next, theoretical reflectance curves for multi layer stacks were calculated using the matrix method. In the fitting procedure the calculated curve was compared to the measured curve. As a result of the fitting, complex refractive index of the QW material was obtained. The growth rates of the layers were fixed by determining the growth rates from the layer thicknesses obtained by HR-XRD. Also the complex refractive index of GaAs was fixed to the previously measured value.

The real and imaginary parts of the complex refractive index of InGaAs(N) were found to be linearly dependent on the indium content over the nitrogen content range studied. Also the imaginary part of the complex refractive index of (In)GaAsN was found to be linearly dependent on the nitrogen content. However, the real part of the complex refractive index of (In)GaAsN did not change as a function of the nitrogen content. These dependencies are important for the in situ determination of the QW composition by matrix method simulations. When ternary alloy InGaAs is considered, the imaginary part of the complex refractive index is preferable over the real part for composition determination because it is more sensitive to the changes of the indium content. When GaAsN is considered, the imaginary part must be utilised because the real part does not depend on the nitrogen content.

The determination of the composition of the quaternary alloy InGaAsN is also possible using in situ reflectance curve measured during growth of the MQW structure. Because the real part of the complex refractive index of InGaAsN is not affected by the nitrogen content, the real part can be used to determine the indium content of the sample. After that, the nitrogen content of the QWs can be determined from the imaginary part of the complex refractive index.

The results obtained from in situ monitoring of MQW structures were promising. However, improvements in the measurement system need to be done in order to make the determination of the composition more accurate and to enable the use of this method in commercial monitoring. In addition, the possibility to obtain both the composition and the growth rate *in situ* from the reflectance curve should be studied carefully. As a final goal, a feedback loop between the in situ measurement and analysis and the MOVPE growth control system could be envisaged, so that the data obtained during growth would be used to adjust the growth parameters in real time.

References

[1] M. A. Herman, W. Richter and H. Sitter, *Epitaxy, Physical principles and technical implementation* (Springer-Verlag, Berlin Heidelberg, 2004).

[2] I. Akasaki, H. Amano, Y. Koide, K. Hiramatsu and N. Sawaki, J. Cryst. Growth **98**, 209 (1989).

[3] N. C. Frateschi, S. G. Hummel and P. D. Dapkus, Electronics Letters **27**, 155 (1991).

[4] Y. Raffle, R. Kuszelewicz, R. Azoulay, G. Le Roux, J. C. Michel, L. Dugrand and E. Toussaere, Appl. Phys. Lett. **63**, 3479 (1993).

[5] C. Watatani, Y. Hanamaki, M. Takemi, K. Ono, Y. Mihashi and T. Nishimura, J. Cryst. Growth **281**, 227 (2005).

[6] W. G. Breiland and K. P. Killeen, J. Appl. Phys. **78**, 6726 (1995).

[7] J.-H. Baek, B. Lee, S. W. Choi, J. H. Lee and E.-H. Lee, Appl. Phys. Lett. **68**, 2355 (1996).

[8] J.-H. Baek, B. Lee, W. S. Han, H. K. Cho, J. M. Smith and I. H. Choi, Jpn. J. Appl. Phys. **38**, 2707 (1999).

[9] R. M. Lum, M. L. McDonald, J. C. Bean, J. Vandenberg, T. L. Pernell and S. N. G. Chu, Appl. Phys. Lett. **69**, 928 (1996).

[10] M. Zorn, K. Haberland, A. Knigge, A. Bhattacharya, M. Weyers, J.-T. Zettler and W. Richter, J. Cryst. Growth **235**, 25 (2002).

[11] P. Wolfram, E. Steimetz, W. Ebert, B. Henninger and J.-T. Zettler, J. Cryst. Growth **248**, 240 (2003).

[12] M. Kondow, K. Uomi, A. Niwa, T. Kitatani, S. Watahiki and Y. Yazawa, Jpn. J. Appl. Phys. **35**, 1273 (1996).

[13] W. Shan, W. Walukiewicz, K. M. Yu, J. Wu, J. W. Ager III, E. E. Haller, H. P. Xin and C. W. Tu, Appl. Phys. Lett. **76**, 3251 (2000).

[14] J. N. Baillargeon, K. Y. Cheng, G. E. Hofler, P. J. Pearah and K. C. Hsieh, Appl. Phys. Lett. **60**, 2540 (1992).

[15] W. G. Bi and C. W. Tu, Appl. Phys. Lett. **69**, 3710 (1996).

[16] W. G. Bi and C. W. Tu, J. Appl. Phys. **80**, 1934 (1996).

[17] W. Shan, K. M. Yu, W. Walukiewicz, J. W. Ager III, E. E. Haller and M. C. Ridgway, Appl. Phys. Lett. **75**, 1410 (1999).

[18] B. Kunert, K. Volz, J. Koch and W. Stolz, Appl. Phys. Lett. **88**, 182108 (2006).

[19] M. Le Du, J.-C. Harmand, K. Meunier, G. Patriarche and J.-L. Oudar, IEE Proc.-Optoelectron. **151**, 254 (2004).

[20] W. G. Bi and C. W. Tu, Appl. Phys. Lett. **70**, 1608 (1997).

[21] K. Volz, O. Rubel, T. Torunski, S. D. Baranovskii and W. Stolz, Appl. Phys. Lett. **88**, 081910 (2006).

[22] I. Vurgaftman, J. R. Meyer and L. R. Ram-Mohan, J. Appl. Phys. **89**, 5815 (2001).

[23] S.-H. Wei and A. Zunger, Phys. Rev. Lett. **76**, 664 (1996).

[24] U. Tisch, E. Finkman and J. Salzman, Appl. Phys. Lett. **81**, 463 (2002).

[25] W. Shan, W. Walukiewicz, J. W. Ager III, E. E. Haller, J. F. Geisz, D. J. Friedman, J. M. Olson and S. R. Kurtz, Phys. Rev. Lett. **82**, 1221 (1999).

[26] W. Shan et al., phys. stat. sol. b **223**, 75 (2001).

[27] J. Wu, W. Shan and W. Walukiewicz, Semic. Sci. Techn. **17**, 860 (2002).

[28] P. R. C. Kent and A. Zunger, Phys. Rev. Lett. **86**, 2613 (2001).

[29] P. R. C. Kent and A. Zunger, Phys. Rev. B **64**, 115208 (2001).

[30] E. P. O'Reilly and A. Lindsay, phys. stat. sol. b **216**, 131 (1999).

[31] L. Bellaiche, S.-H. Wei and A. Zunger, Phys. Rev. B **54**, 17568 (1996).

[32] I. A. Buyanova, W. M. Chen and M. O. Manasreh, eds., *Physics and application of dilute nitrides* (Taylor & Francis Books, inc., New York, 2004).

[33] A. Lindsay and E. P. O'Reilly, phys. stat. sol. b **216**, 131 (1999).

[34] P. J. Klar, H. Grüning, W. Heimbrodt, J. Koch, W. Stolz, P. M. A. Vicente, A. M. Kamal Saadi, A. Lindsay and E. P. O'Reilly, phys. stat. sol. b **223**, 163 (2001).

[35] T. Kitatani, M. Kondow, T. Kikawa, Y. Yazawa, M. Okai and K. Uomi, Jpn. J. Appl. Phys. **38**, 5003 (1999).

[36] S. Sakai, Y. Ueta and Y. Terauchi, Jpn. J. Appl. Phys. **32**, 4413 (1993).

[37] S. A. Ding, S. R. Barman, K. Horn, H. Yang, B. Yang, O. Brandt and K. Ploog, Appl. Phys. Lett. **70**, 2407 (1997).

[38] I. A. Buyanova, W. M. Chen and C. W. Tu, Semic. Sci. Techn. **17**, 815 (2002).

[39] J. F. Geisz, D. J. Friedman, J. M. Olson, S. R. Kurtz and B. M. Keyes, J. Cryst. Growth **195**, 401 (1998).

[40] S. R. Kurtz, A. A. Allerman, C. H. Seager, R. M. Sieg and E. D. Jones, Appl. Phys. Lett. **77**, 400 (2000).

[41] N. Q. Thinh, I. A. Buyanova, W. M. Chen, H. P. Xin and C. W. Tu, Appl. Phys. Lett. **79**, 3089 (2001).

[42] S. G. Spruytte, C. W. Coldren, J. S. Harris, W. Wampler, P. Krispin, K. Ploog and M. C. Larson, J. Appl. Phys. **89**, 4401 (2001).

[43] J. Toivonen, T. Hakkarainen, M. Sopanen, H. Lipsanen, J. Oila and K. Saarinen, Appl. Phys. Lett. **82**, 40 (2003).

[44] W. Li, M. Pessa, T. Ahlgren and J. Decker, Appl. Phys. Lett. **79**, 1094 (2001).

[45] A. Ptak, S. Kurtz, M. Weber and K. Lynn, J. Vac. Sci. Technol. B **22**, 1584 (2004).

[46] Y. Shimizu, Y. Mura, A. Uedono and Y. Okada, J. Appl. Phys. **100**, 064910 (2006).

[47] A. Janotti, S. H. Wei, S. B. Zhang, S. Kurtz and C. G. Van de Walle, Phys. Rev. B **67**, 161201 (2003).

[48] A. J. Ptak, S. W. Johnston, S. Kurtz, D. J. Friedman and W. K. Metzger, J. Cryst. Growth **251**, 392 (2003).

[49] G. Baldassarri H. v. H., M. Bissiri, A. Polimeni, M. Capizzi, M. Fischer, M. Reinhardt and A. Forchel, Appl. Phys. Lett. **78**, 3472 (2001).

[50] A. Janotti, S. B. Zhang, S. H. Wei and C. G. Van de Walle, Optical Materials **25**, 261 (2004).

[51] E. V. K. Rao, A. Ougazzaden, Y. Le Bellego and M. Juhel, Appl. Phys. Lett. **72**, 1409 (1998).

[52] J. Toivonen, T. Hakkarainen, M. Sopanen and H. Lipsanen, IEE Proc. Optoel. **150**, 68 (2003).

[53] J. Toivonen, T. Hakkarainen, M. Sopanen and H. Lipsanen, J. Cryst. Growth **221**, 456 (2000).

[54] K. Volz, J. Koch, B. Kunert, I. Nemeth and W. Stolz, J. Cryst. Growth **298**, 126 (2007).

[55] T. Hakkarainen, J. Toivonen, M. Sopanen and H. Lipsanen, J. Cryst. Growth **234**, 631 (2002).

[56] K. Volz, T. Torunski, B. Kunert, O. Rubel, S. Nau, S. Reinhard and W. Stolz, J. Cryst. Growth **272**, 739 (2004).

[57] O. Rubel, K. Volz, T. Torunski, S. D. Baranovskii, F. Grosse and W. Stolz, Appl. Phys. Lett. **85**, 5908 (2004).

[58] P. J. Klar, H. Grüning, J. Koch, S. Schäfer, K. Volz, W. Stolz, W. Heimbrodt, A. M. Kamal Saadi, A. Lindsay and E. P. O'Reilly, Phys. Rev. B **64**, 121203 (2001).

[59] K. Kim and A. Zunger, Phys. Rev. Lett. **86**, 2609 (2001).

[60] M. Kondow, T. Kitatani, S. Nakastsuka, M. C. Larson, K. Nakahara, Y. Yazawa, M. Okai and K. Uomi, IEEE J. Selected Topics in Quantum Electr. **3**, 719 (1997).

[61] C. Ellmers, F. Höhnsdorf, J. Koch, C. Agert, S. Leu, D. Karaiskaj, M. Hofmann, W. Stolz and W. W. Rühle, Appl. Phys. Lett. **74**, 2271 (1999).

[62] G. Steinle, H. Riechert and A. Y. Egorov, Electr. Lett. **37**, 93 (2001).

[63] A. Y. Egorov et al., J. Cryst. Growth **227–228**, 545 (2001).

[64] S. R. Kurtz, A. A. Allerman, E. D. Jones, J. M. Gee, J. J. Banas and B. E. Hammons, Appl. Phys. Lett. **74**, 729 (1999).

[65] D. J. Friedman, J. F. Geisz, S. R. Kurtz and J. M. Olson, J. Cryst. Growth **195**, 409 (1998).

[66] O. G. Okhotnikov, T. Jouhti, J. Konttinen, S. Karirinne and M. Pessa, Opt. Lett. **28**, 364 (2003).

[67] S. Schön, A. Rutz, V. Liverini, R. Grange, M. Haiml, S. C. Zeller and U. Keller, J. Cryst. Growth **278**, 239 (2005).

[68] G. B. Stringfellow, *Organometallic Vapor-Phase Epitaxy: Theory and Practice* (Academic Press, Inc., San Diego, 1989).

[69] C. A. Larsen, N. I. Buchan, S. H. Li and G. B. Stringfellow, J. Cryst. Growth **102**, 103 (1990).

[70] E. Bourret-Courchesne, Q. Ye, D. W. Peters, J. Arnold, M. Ahmed, S. J. C. Irvine, R. Kanjolia, L. M. Smith and S. A. Rushworth, J. Cryst. Growth **217**, 47 (2000).

[71] D. J. Friedman, A. G. Norman, J. F. Geisz and S. R. Kurtz, J. Cryst. Growth **208**, 11 (2000).

[72] S. Kurtz, R. Reedy, G. Barber, J. Geisz, D. Friedman, W. McMahon and J. Olson, J. Cryst. Growth **234**, 318 (2002).

[73] A. J. Ptak, S. Kurtz, C. Curtis, R. Reedy and J. Olson, J. Cryst. Growth **243**, 231 (2002).

[74] J. Derluyn, I. Moerman, M. R. Leys, G. Patriarche, G. Sek, R. Kudrawiec, W. Rudno-Rudzinski, K. Ryczko and J. Misiewicz, J. Appl. Phys. **94**, 2752 (2003).

[75] T. Miyamoto, T. Kageyama, S. Makino, D. Schlenker, F. Koyama and K. Iga, J. Cryst. Growth **309**, 339 (2000).

[76] A. Moto, M. Takahashi and S. Takagishi, J. Cryst. Growth **221**, 485 (2000).

[77] D. J. Friedman, J. F. Geisz, S. R. Kurtz, J. M. Olson and R. Reedy, Journal of Crystal Growth **195**, 438 (1998).

[78] R. Bhat, C. Caneau, L. Salamanca-Riba, W. Bi and C. Tu, J. Cryst. Growth **195**, 427 (1998).

[79] S. B. Zhang and A. Zunger, Appl. Phys. Lett. **71**, 677 (1997).

[80] I. Suemune, K. Uesugi and T.-Y. Seong, Semic. Sci. Techn. **17**, 755 (2002).

[81] A. Ougazzaden, E. Rao, B. Sermage, L. Leprince and M. Gauneau, Jpn. J. Appl. Phys. **38**, 1019 (1999).

[82] A. Ougazzaden, Y. Le Bellego, E. V. K. Rao, M. Juhel, L. Leprince and G. Patriarche, Appl. Phys. Lett. **70**, 2861 (1997).

[83] F. Höhnsdorf, J. Koch, C. Agert and W. Stolz, J. Cryst. Growth **195**, 391 (1998).

[84] F. Höhnsdorf, J. Koch, A. Hasse, A. Schaper, W. Stolz, C. Giannini and L. Tapfer, Physica E **8**, 205 (2000).

[85] L. E. Tarof, C. J. Miner and C. Blaauw, J. Appl. Phys. **68**, 2927 (1990).

[86] A. Rebey, M. M. Habchi, A. Bchetnia and B. El Jani, J. Cryst. Growth **261**, 450 (2004).

[87] A. Rebey, M. M. Habchi, Z. Benzarti and B. El Jani, Microel. J. **35**, 179 (2004).

[88] D. E. Aspnes, S. M. Kelso, R. A. Logan and R. Bhat, J. Appl. Phys. **60**, 754 (1986).

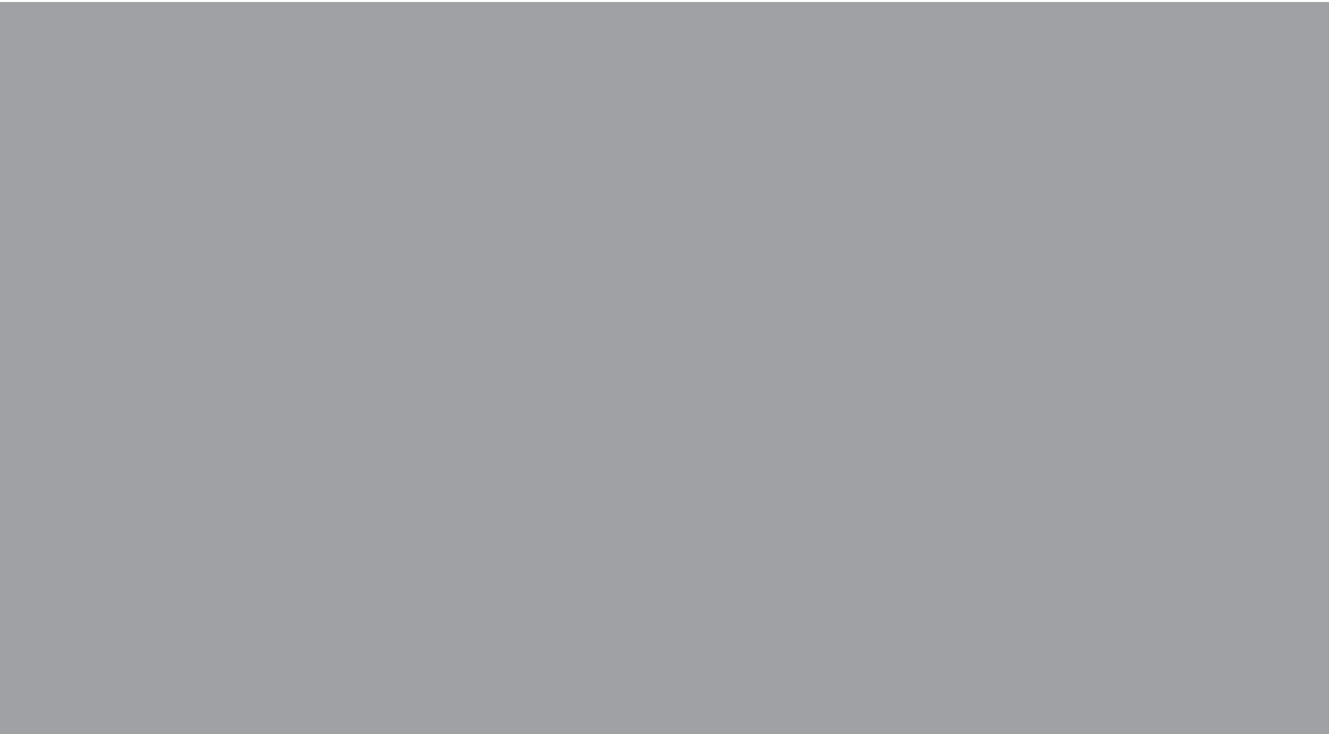

ISBN 978-951-22-8730-7
ISBN 978-951-22-8731-4 (PDF)
ISSN 1795-2239
ISSN 1795-4584 (PDF)